HOW DOES THE WWE DOMAIN OF PARP13 REGULATE THE ASSEMBLY OF STRESS GRANULES?

by
Shang-Jung Cheng

A thesis submitted to Johns Hopkins University in conformity with the requirements for the degree of Master of Science

Baltimore, Maryland
August, 2017

Abstract

Stress granules (SGs) are cytoplasmic mRNA-protein complexes (mRNPs) that form when cells undergo protein translation arrest induced by intrinsic or extrinsic stress. The assembly of SGs is controlled by many factors, including weak electrostatic interactions between proteins and repeating units of RNAs. Structurally, another polynucleotide known as poly(ADP-ribose) (PAR) possesses similar features as RNA; however, the regulation of PAR on SGs remain elusive. Previously, it is known that PAR, five PAR polymerases (PARP), including PARP-13, and two isoforms of PAR glycohydrolase are localized in SGs, implicating that PAR is crucial for SG's maintenance. Here, we decipher how PARP-13 contributes to SG assembly. First, we found that the WWE domain of PARP-13 is sufficient for SG co-localization. Given that the most well studied WWE domain in RNF-146 is able to bind to *iso*-ADP-ribose, which is the minimal structural unit of PAR, we were curious whether the domain in PARP-13 shares similar binding ability. From sequence alignment, we chose two amino acid residues, Y659 and Q668, of PARP-13 for mutation, which are conserved between PARP-13 and RNF146 and essential for PAR binding in RNF-146. Immunofluorescence data demonstrated that expression of PARP-13 Y659A mutant generated a higher number and smaller size of SGs while Q668A mutant caused intermediate number and size of SGs compared to the wild-type. Such fragmented SGs were also observed in both HeLa $(K)^{PARP13-/-}$ and U2OS cells when overexpressing these PARP-13 mutants, implicating that the phenotype is not limited to specific cell types. Based on these observations, we hypothesize that PARP-13-WWE can bind to PAR, which provides as a scaffold to bridge RNA/protein complexes and promote the formation of bigger SGs while the mutants of which lack this PAR-

protein interaction makes SG fragmentation. To test the hypothesis, we performed an *in vitro* PAR binding assay and identified that PARP-13-WWE along with zinc finger domain binds to PAR in a dose-dependent manner. The PAR-binding ability of PARP-13 mutants are under active investigation. In addition, we found that wild-type and fragmented SGs due to the expression of PARP-13 WWE mutant display different biophysical properties, that the wild-type granules disappear after 1,6-hexanediol treatment, and the mutant ones remain in the cytoplasm. Taken together, we demonstrated that WWE of PARP-13 with zinc finger domain is able to bind to PAR and facilitate the formation of bigger SGs. Mutation of Y659 and Q668 on WWE domain changes physical properties of SGs, suggesting that the dynamics of SGs could be modulated by PAR.

Thesis advisor: Dr. Anthony K.L. Leung

Thesis secondary reader: Dr. Michael J. Matunis

Acknowledgements

It takes a village to see a completion of a project. I would like to thank Dr. Anthony Leung, my thesis mentor, for making me a member of his lab and providing constant encouragement. His optimism and passion toward science motivate me to push boundaries while doing research and give me the courage pursuing my professional aspirations bravely. I would like to express my gratitude to my secondary reader, Dr. Michael Matunis, who constantly provides constructive pointers and encouragement during our meetings. I have benefited greatly from Dr. Jennifer Kavran‘s elucidation on selecting appropriate site supporting stable DNA structure during the protein purification. Without her input, this project would not be possible.

Dr. P.C. Huang shows empathy and understanding especially during my first year in a foreign country and a challenging curriculum. Thanks to his generosity and warmness, I was able to brave through various difficulties and discover my potentials. The research process can be arduous, but thanks to all my lab members who foster a friendly and collegial environment, we can share moments of levity, as well as solving problems and sharing ideas together. Lastly, I want to thank Tien-Fu Cheng, Yu-Hua Chen, and Shangching Cheng, my nagging yet loving family for all the support. You gave me the courage to persevere and to chase my dream, and now, I would like to share all the honors with you.

Table of contents **Page references**

List of Tables **Page references**

List of Figures **Page references**

Chapter I

Introduction

I, Stress granules

(1) What are stress granules?

In order to survive, organisms have developed different strategies to adapt to adverse environment. The formation of stress granules is one of them, which could be found in nematodes, fruit flies, yeast, plants and mammals [1, 2]. Stress granules are non-membranous cytoplasmic foci consisting of mRNA and proteins, range from 0.4 to 5 μm, and are induced by stalled protein translation initiation under stress [3]. A variety of stresses could stimulate the formation of stress granules, including UV, heat shock, oxidative stress, hypoxia, glucose deprivation, and viral infection. To deal with stress, translating initiation machinery is repressed, which in turn increases free mRNA in the cytoplasm and favors the assembly of stress granules. On the other hand, stabilizing mRNA with polysome shifts the balance to stress granule disassembly, implicating that the amount of free mRNA accumulation determines the kinetics of stress granule formation [4]. Arrest of translation initiation could be achieved via two mechanisms. The first canonical pathway takes place through phosphorylation of eukaryotic initiation factor 2 (eIF2α) at Serine 51. Under normal condition, eIF2 is able to assemble to eIF2/GTP/Met-tRNAi^{Met} ternary complex that delivers tRNA to 40S ribosome and recognize AUG start codon on the 5'-end of mRNA for translation. Phosphorylation of eIF2α at S51 reduces its GTP/GDP exchange ability and lowers the level of competent ternary complex for translation, resulting in global decrease on protein synthesis [5, 6]. Stalled 48S pre-initiation complex with selective components, such as eIF3 and poly $(A)^+$

RNA, will be recruited to form stress granules [7]. The other non-canonical pathway for stress granule formation is via cap-binding eIF4F complex. The eIF4F complex is composed of a cap-binding protein eIF4E, RNA helicase eIF4A, and scaffold molecule eIF4G. eIF4G not only links eIF4E and eIF4A, but also interacts with ribosome binding factor-eIF3 and poly(A)-binding proteins, bridging the association between ribosome and mRNA [8, 9]. Disrupting eIF4F complex, either via depriving eIF4E molecule from the complex by eIF4E-binding proteins (4E-BPs) or inhibiting activities of individual component in eIF4F complex, such as inhibiting helicase or ATPase activities of eIF4A, will decrease protein translation and induce stress granules [10]. Both pathways serve as checkpoints to determine protein translation as well as stress granule formation.

(2) Composition of stress granules

Stress granules were triggered by stalled protein translation initiation; therefore, the fundamental composition of stress granules is made up of mRNA with poly (A) tail, eukaryotic translation initiation factors, poly (A)-binding protein (PABP) 1, and small ribosomal subunits. In addition to the above components, which situated in the core region of stress granules, various kinds of RNA-binding proteins (RBPs) have been characterized as stress granule components through RNA-protein interactions. Most of the RBPs are able to regulate mRNA, including mediating mRNA translation, splicing, or stability [11]. For example, the common stress granule marker, T cell internal antigen-1 (TIA-1) has been demonstrated to modulate alternative splicing of fibroblast growth factor receptor 2 (FGFR-2) by promoting K-SAM exon inclusion [12]. It is noteworthy to mention that several RBPs, which contain prion-like domains (PLD) or poly glycine-rich

domain, tend to form aggregates even without stress stimulation. The self-aggregation property of RBPs facilitate the recruitment of other proteins to stress granules via protein-protein interactions [13]. Those recruited proteins might not function as RNA regulator; instead, they are involved in critical signaling pathways, suggesting the potential roles of stress granule in signaling cross-talks [14]. For instance, receptor for activated C kinase 1 (RACK1) is able to induce apoptosis by suppressing Src activation [15]. Sequestering RACK1 to stress granules could prevent it from participating apoptosis pathway and contribute to anti-apoptosis. Identification of these proteins broadens our scope toward stress granules' proposed functions. Although stress granules induced by different stresses share common factors, it is known that some constituents are distinct corresponding to stress types. For example, Sam68, one of the RBPs, could be found in stress granules during poliovirus infection, but not in those granules induced by heat shock or UV irradiation [16]. In addition, several kinds of post-translational modifications (PTMs) of stress granule proteins have been identified as regulators for stress granule's assembly and functions, including phosphorylation, O-GlcNAcylation, methylation, and hypusination [17]. Different PTMs on the same crucial components of stress granules play different roles on stress granule assembly. Taken Ras-GAP SH3-binding protein 1 (G3BP1) as an example, methylation of arginine residue on RGG domain prevents stress granule assembly [18] while phosphorylation on serine 149 stimulates its oligomerization as well as stress granule assembly [19]. It implicates that PTMs could fine-tune the dynamics of stress granules. The high dynamicity as well as varying participating molecules suggest that stress granules are able to modulate cellular functions so as to adapt to environmental signaling changes in a specific way [3].

(3) Assembly and disassembly of stress granules

The assembly of stress granules is a step-wise process [10]. First, translation initiation complex dissociates from polysome during translation arrest. At the same time, the accumulation of RNA-binding proteins with PLD or low complexity domain (LCD) of which recruited to the complex via RNA-protein interaction are able to form aggregates spontaneously. The oligomerization serves as a stable "core" to nucleate stress granules [20]. In addition, proteins with LCD possess specific repeated amino acid composition and flexible conformation, which could further drive liquid-liquid phase separation (LLPS) by mediating physical interactions, such as weak electrostatic interactions and hydrophobic protein-protein interactions. It is noteworthy to mention that several PTMs could modulate conformation of LCD [21], and further impact stress granule assembly. The phase separation could be enhanced by other physical factors in the environment, including salt concentration, molecular crowding, charge valency and temperature [22]. LLPS in the cytoplasm is able to attract more molecules to form a less-condensed dynamic "shell" around the "core" of stress granules. The biphasic structures could fuse together initially in an ATP-dependent way [23]. Microtubule transport, which happened later, could make the nanoscopic stress granules grow to microscopical visible ones, to achieve mature size of stress granules [10, 24]. The formation of stress granules is a reversible process. Once the stress is relieved, stress granules disassemble, and the stalled mRNA transcripts either recover to translation or undergo degradation [2]. There were two mechanisms proposed for the clearance of stress granules. The first one is by chaperon-mediated disaggregation. It is reported that chaperon HSP70 complex with

HSPB8 and BAG3 is able to dissolve misfolded proteins in mammalian stress granules to ensure in-time disassembly. In addition, HSPB1 works coordinately later to prevent the formation of irreversible aggregates [25]. The other one is by autophagy. From the gene screen in yeast, it is identified that stress granules could be targeted to granuolophagy, a specific way of autophagy [26]. Another study indicated that the disassembly of stress granules is similar as the inverse steps of assembly, where the components in less-condensed "shell" dissolve faster than the stable "core" [22]. The observation of longer lifetime of "core" structure was suggested as a protecting mechanism that enables cell to respond efficiently if re-encounter stress [10].

(4) Proposed functions of stress granules

Given the characteristics that stress granules were tightly regulated by the presence of stalled protein translation initiation complex, the proposed function of stress granules was originally regarded as a temporary spot for non-translating mRNA storage. However, emergent evidence indicate that components in stress granules are not static. Instead, the shuttling of components, including proteins and mRNA transcripts, in and out of stress granules have been observed in fluorescence recovery after bleaching (FRAP) experiments. These observations implied that the role of stress granules' might not likely to be repositories containing translational silenced mRNAs [7]. Based on its high dynamics, it is proposed that stress granules could act as an mRNA triage [27, 28]. By exchanging components with polysomes and P-bodies, stress granules could determine the priority of which mRNA transcripts to be translated or degraded corresponding to the environment [3]. Additionally, identification of signaling molecules as stress granule

components expanded our knowledge to stress granules' functions. One of the most well-studied signaling pathways is apoptosis. Many pieces of evidence have demonstrated that stress granules regulate apoptosis through different pathways. For instance, stress granules could sequester RACK1 from cytosol to inhibit MAP kinase and conquer apoptosis [29]. During stress, astrin recruits raptor molecules to stress granules from mTORC1 pathway, and lowers mTORC1-hyperactivation-induced apoptosis [30]. Oxidizing cysteine 36 of TIA-1, one of the main stress granule proteins, triggers stress granule inhibition as well as apoptosis [31]. Even though the actual functions of stress granules remain elusive, it is likely that stress granules enable cells to deal with emergent endogenous/exogenous changes and maintain physiological homeostasis or survival.

II, Poly-ADP-ribose (PAR)

(1) What is Poly-ADP-ribose?

Poly-ADP-ribose is a polymer that consists of two or more ADP-ribose units. The long-chain structure could be synthesized in either linear or branched form. For both linear and branch structures, ADP-ribose is conjugated to the adjacent non-adenosine subunit via $\alpha(1\rightarrow2)$ ribose-ribose glycosidic bond [32]. ADP-ribosylation—transferring one or more ADP-ribose units from nicotinamide adenine dinucleotide (NAD^+) onto amino acid residues by poly-ADP-ribose polymerases (PARPs)—is one of the most important PTMs. The covalent modification has been found in specific amino acids, such as aspartate, glutamate, arginine, lysine, and serine residues [33]. The length of PAR on modification ranges from short ones up to 200 subunits, from linear ones to branched ones, providing structure complexity as well as diverse functions [34]. Evidence have

shown that ADP-ribosylation modulates many crucial cellular signaling pathways, such as DNA repair, transcriptional regulation, and stress response [35].

(2) Poly-ADP-ribose polymerase (PARPs) family proteins

Poly(ADP-Ribosyl)ation (PARylation) was regulated by a specific family of enzymes termed as ADP-ribosyltransferses, or commonly known as poly(ADP-ribose) polymerases (PARPs). There are 17 PARPs identified in humans with distinct classes of catalytic activity [36]—some of them add multiple ADP-ribose subunits on protein substrates (PARylation), including PARP-1, PARP-2, PARP-3, PARP-4, PARP-5a and PARP-5b while some add only one ADP-ribose in each modified residue (MARylation), including PARP-6, PARP-7, PARP-8, PARP-10, PARP-11, PARP-12, PARP-14, PARP-15, and PARP-16 [36-38]. Among the family, PARP-9 and PARP-13 were identified as catalytically inactive. The enzymatic activity was determined by amino acid composition of the catalytic center on the PARP domain. The catalytic binding pocket, H(Histidine)-Y(Tyrosine)-E(Glutamate) triad, on PARP domain coordinates with NAD^+ positioning for correct orientation of PARylation [39]. For enzymes possess PARylating activity, the glutamate residue on the triad could activate additional cofactor NAD^+ to acceptor residues and render PAR chain elongation [39]. On the other hand, MARylating enzymes, as shown in the case of PARP-10, can utilize glutamate residue from substrate to stabilize oxocarbenium intermediate and activate NAD^+, since the catalytic domain lacks glutamate residue. Therefore, the substrate-assisted activation lost ability after its modification, limiting the modification to single ADP-ribose [40]. For PARP-9 and PARP-13, both protein families appear to lose the conserved H-Y-E motif. Given that the

lack of the structural requirement for NAD^+ binding, they were categorized as catalytically inactive PARPs [41, 42]. PARylation is a reversible process, and there are several enzymes were able for the degradation. Poly(ADP-ribose) glycohydrolase (PARG) is able to cleave the glycosidic ribose-ribose bond within PAR back to the mono-ADP-ribosylated state [43]. Another enzyme that studied to cleave PAR is ADP-ribosylhydrolase 3 (ARH3), but the specificity is lower than PARG. Studies have demonstrated that ARH3 is able to hydrolyze both PAR and O-acetyl-ADP-ribose, one of the metabolites from NAD^+-dependent deacetylase pathway [44]. Recently, it is found that ARH3 is capable to remove ADP-ribose from serine-ribosylated substrates specifically [45]. Apart from the above enzymes, there were three enzymes have been identified as reversing PARP-dependent MARylation—MacroD1, MacroD2, and terminal ADP-ribose glycohydrolase 1 (TARG1) [43]. Cooperating together, PARPs and degrading enzymes are able to keep appropriate level of ADP-ribosylation in cells.

(3) PAR recognition domains

In addition to poly(ADP-ribose) binding proteins, the repetitive and multivalent features of PAR enables it to interact with other molecules non-covalently [46]. It is known that the adenosine of PAR is potential to undergo base stacking as well as hydrogen bonding. Besides, each subunit of PAR contains pyrophosphate linkage, renders the structure high anionic charges. Early study had demonstrated that the polynucleotide serves as reaction platform to coordinate molecules together during DNA-damage response [47]. In recent years, proteomic studies have identified proteins of which associated with PAR either by covalently PARylation or noncovalently PAR-

binding [48]. Apart from that, several PAR-binding modules have been identified [37]. Characteristics for these modules are variable. The size ranges from 20-190 residues, and the structure differs from folded to disordered sequences, implicating that they could fit specific cellular function in need. PAR-binding motifs (PBMs) were the first discovered module for PAR binding. The small motif, which is ranging from 20-25 residues with positive charges, was proposed to interact with PAR electrostatically with high affinity. The main function of PBMs was carrying proteins to sites of PARylation, especially during PARP-1-activation under DNA damage [43]. Another motif of which is common for recognizing nucleic acid is zinc fingers, and PAR-binding zinc fingers (PBZs) have been found in specific proteins regulating DNA repair or cell cycle checkpoint [49]. Biochemical and structural studies identified that C2-H2 type of PBZ binds to PAR by recognizing two consecutive ADP-ribose moieties. Moreover, tandem PBZs are able to cooperate together and make the PAR-binding with higher affinity, such as aprataxin PNK-like factor (APLF) [37]. In addition to small motifs, macrodomain has demonstrated that PAR binding domain could be in bigger size, which range from 130-190 residues [37]. Both monomeric and polymeric ADP-ribose bind to macrodomain, since macrodomain recognizes terminal ADP-ribose with high affinity by forming multiple noncovalent interactions with distal ribose and two phosphate groups of ADP-ribose [50]. The features of macrodomain do not limited to PAR-binding, but also possess mono-ADP-ribosylhydrolase activity, as in the case for MacroD1 and MacroD2 [51]. Interestingly, studies have indicated the subtle variance on the macrodomain sequences contribute to different catalytic activity from binding to removing [37]. Another example is WWE domain. The domain was named after the most conserved

amino acids— two tryptophan and a glutamate residues [52]. The globular module was present in two specific protein families, ubiquitin E3-ligase, such as RNF-146 and HUWE1, and PARP family proteins, including PARP-7,-11,-12,-13, and-14. The most well-characterized WWE is from RNF-146. Demonstrated by X-ray crystallography, WWE domain of RNF-146 binds to *iso*-ADP-ribose, which is the smallest structural unit within PAR [53]. The two separated ribose-phosphate groups of *iso*-ADP-ribose fit the structure of WWE domain and form an extensive interaction [53]. Moreover, the functions of RNF-146 are well studied, that it could catalyze PAR-dependent ubiquitination on protein targets to mediate proteasome degradation [37]. For those WWE domains in PARP protein family, the structures and functions are not totally understood. Based on similar structures, some studies mentioned that PAR could be recognized by some RNA-recognition motifs (RRMs) by potential electrostatic interactions, such as hnRNP proteins [37]. Therefore, it is proposed that PAR could compete for the same substrate over RNA by attracting RNA-binding proteins to sites of PARylation [43].

(4) Involvement of PAR to stress granules

The regulation of PAR in the nucleus during DNA damage, chromosome segregation, and transcription has been widely investigated. In recent years, it is demonstrated that PAR also modulates post-transcriptional gene expression in cytoplasm during stress. Most of the PARPs are cytoplasmic [54]. In addition, PAR is critical for stress granule assembly in cytoplasm [55]. When there is no stress, PARPs were dispersed in the cytoplasm; during stress condition, six PARPs co-localize with stress

granules, including PARP-5a, PARP-12, PARP-13.1, PARP-13.2, and PARP-14 and PARP-15. Moreover, two PARG isoforms—PARG99 and PARG102, have been identified to co-localize with stress granules. The presence of both synthesizing and degrading enzymes of PAR in stress granules suggests that the assembly and disassembly could be regulated by PAR. Besides, PAR could covalently modify substrate proteins, such as RNA binding proteins, to fine-tune the interaction with mRNA. [35]

III, PARP13

(1) Domain constituents and studied functions

Of all stress granule PARPs, PARP-13 is the only protein without ADP-ribosylating activity. It is because of the conserved H-Y-E triad on PARP domain is replaced by Y-Y-V residues, which lacks the required glutamate residue for NAD^+ binding [41]. There are two isoforms of PARP13—PARP-13.1 and PARP-13.2. The only difference is that PARP-13.1 carries the PARP-like domain on the C-terminus (Fig. 1a). PARP13, which also termed as Zinc finger Anti-viral Protein (ZAP), binds to viral mRNA transcripts via CCCH-type zinc-fingers on the N-terminus and leads to mRNA degradation and delayed replication [56]. Specific categories of RNA viruses are identified as targets of PARP-13, including HIV-1, alphaviruses and filoviruses. Evidence also indicated that PARP-13.2 binds to innate immune response factor, RIG-I, after viral infection [57]. Taken together, PARP-13 is able to mediate host factors and resist viral infection. In addition to the abovementioned domains, PARP-13 also contains WWE domain, which is proposed as a PAR-binding motif. Even though the structure and exact functions of the domain remain unclear, we have noticed that many PARPs with

WWE domain are also localized in stress granules, including PARP-12 and PARP-14, suggesting that WWE might be critical in regulating stress granules formation— a focus of this thesis.

(2) Proposed mechanism of how PARP-13 regulates stress granule assembly

Given that PARP-13 co-localizes with stress granules during stress condition, it is not clear whether and, if so, how the catalytically inactive PARP regulates stress granules. Based on the domain features, PARP-13 contains zinc fingers, which is able to bind to mRNA transcript via RNA-protein interaction. Apart from that, the putative PAR binding motif of PARP-13, WWE domain, might be able to incorporate PAR to stress granules and maintain structural integrity. Therefore, we hypothesize that PARP-13 binds to PAR via WWE domain, just as the WWE domain of RNF-146, during stress. Moreover, the repetitive units and multivalency features of PAR could serve as a scaffold to bridge proteins and RNA together and form macromolecular structure [58]. Beside protein-RNA and protein-protein interactions, we proposed here that proteins could be recruited to stress granules through protein-PAR-protein interaction, to facilitate the assembly of stress granules.

Chapter II

Material and Methods

Chemical reagents and antibodies

Details about all chemical reagents and antibodies used in this study have been listed in Table 1 and 2.

Table 1: Reagents

Name	**Brand**	**Prepare method**
DMEM- High glucose	Gibco (11995-065)	
D-PBS (pH 7.4) (1X)	Gibco (10010-023)	
Fetal Bovine Serum-heat inactivated	Gibco (16140071)	
0.25% Trypsin-EDTA (1X)	Gibco (25200-056)	
Geneticin	Invitrogen (10131-035)	Stock is 50 mg/mL, dilute with medium
Lipofectamine-2000-reagent	Invitrogen (11668-019)	
Sodium arsenite solution ($NaAsO_2$)	Fluka Analytical (35000)	Stock is 50 mg/mL, filtered and keep at 4 °C
Paraformaldehyde solution	Electron Microscopy Sciences (15714)	Stock is 32%, dilute with PBS freshly before use
Triton-X-100	Sigma-Aldrich (T8787)	Prepare 10% stock in water
Tween-20	Sigma-Aldrich (P9416)	
DAPI (4',6-diamidino-2-phenylindoledihydrochloride)	Sigma-Aldrich (D9542)	Stock is 10 mM, dilute with ddH_2O
Prolong-Gold Antifade Mountant	Thermo Fisher (P36934)	
LB Broth	Fisher BioReagents (BP1426-2)	25 g in 1L ddH_2O, autoclaved
Ampicillin sodium salt	Sigma-Aldrich (A9518)	Prepare 100 mg/mL stock in sterilized ddH_2O, filtered for use
IPTG (Isopropyl β-D-1-	Boston BioProducts	Prepare 1M stock: 4.75g in

thiogalactopyranoside)	(P806-10)	20 mL sterilized ddH_2O, filtered for use
Poly-D-lysine hydrobromide	Sigma-Aldrich (P7405)	100x poly-D-lysine: 5 mg in 10 mL filtered water 1x poly-D-lysine: dilute with PBS in 1:100
1,6-hexanediol	Sigma-Aldrich (240117)	Dissolve in complete medium and filtered for use

Table 2: Primary antibody/Secondary antibody

Name	**Brand**	**Dilution**
eIF3η (N20)	Santa Cruz (SC-16377)	1:100 (for IF)
Poly-ADP-ribose (PAR)	Trevigen (4336-BPC)	1:1000 (for slot blot)
FLAG-M2	Sigma-Aldrich (F1804)	1:1000 (for WB)
HIS	Sigma-Aldrich (H1029)	1:1000 (for WB)
Cy5 AffiniPure donkey-anti-goat IgG	Jackson ImmunoResearch Laboratories (705-175-147)	1:500 (for IF)
IRDye 800CW goat-anti-rabbit IgG	LI-COR (92632211)	1:20000 (for slot blot)
IRDye 800CW donkey-anti-mouse IgG	LI-COR (92632212)	1:20000 (for WB)

Cell culture and establishment of stable cell line

HeLa (K), HeLa (K)$^{PARP13-/-}$ [57] , and U2OS cells were maintained in DMEM containing 10% fetal bovine serum at 37°C/5% CO_2. For establishing stable cell lines, 3 x 10^5 cells were seeded in a well of the 6-well plate for 24 hours, and transfected with 2.5 μg EGFP-PARP-13.2, Y659A, and Q668A for 18-24 hours. On the next day, transfer cells to 15 cm plate containing 600 μg/mL Geneticin, and maintain for 7-10 days. Once colonies were formed, pick GFP positive colonies under fluorescence microscope, and transfer them to 24-well plate. Maintain all stable cell lines in medium with Geneticin, and expand them when cells reach high confluence.

DNA Constructs

All constructs used for cell transfection contain EGFP tag were prepared previously in the lab, including PARP13.1 (residues 1-902), PARP13.2 (residues 1-699), insert 5 (residues 380-902), insert 8 (residues 380-698), WWE (594-699), PARP13.2-Y659A, PARP13.2-Q668A, and G3BP1. Constructs for protein purification, RNF-146-WWE-FLAG (residues 98-180), GST-FLAG, and PARP13-WWE-FLAG (residues 604-689), were cloned into pSAT1 vector, which contains 6x-His-SUMO tag. pSAT1 vector was digested with AgeI and BamHI restriction enzymes, and inserts were prepared by polymerase chain reaction (PCR). Details of primers were listed on Table 3.

Table 3: DNA constructs

pSAT1-RNF-146-WWE-FLAG Template: EGFP-RNF-146 Primers: forward: 5'-GTGTGTACCGGTGGAATGAATGGTGAATATGCATGGTAT-3' reverse: 5'-CGCGGATCCGCGCTTACTTGTCGTCATCGTCTTTGTAG TCTAGCCTAAGTCCAGCTACTCC-3'
pSAT1-GST-FLAG Template: pGEX-RNF-146 Primers: forward: 5'- GTGTGTACCGGTGGAATGATGTCCCCTATACTAGGTTA-3' reverse: 5'- CGCGGATCCGCGCTTACTTGTCGTCATCGTCTTTGTAG TCTTTTGGAGGATGGTCGCCACC-3'
pSAT1-PARP13-WWE-FLAG (604-689) Template: EGFP-PARP13.2 Primers: forward: 5'-GTGTGTACCGGTGGAATGACCACCAAATGGATTTGGTATT GG-3' reverse: 5'- CGCGGATCCGCGCTTACTTGTCGTCATCGTCTTTGTAGTCC CACTGAGGCACAAATGTTG-3'

Immunofluorescence

Seed 3x10^5 HeLa (K), HeLa (K)$^{PARP13-/-}$, or U2OS cells in a well of 6-well plate for 24 hours, each well contains 4 coverslips pre-sterilized with 100% ethanol. On the next day, transfect with 2.5 μg corresponding plasmids by Lipofectamin-2000 for 18-24 hours. Stress was induced by100, 250, or 500 μM sodium arsenite in complete DMEM

for 30 or 60 minutes. At the indicated timepoints, rinse coverslips with PBS for 3 times, and fix cells by 4% paraformaldehyde for 10 minutes. Permeabilize cells with 1% Triton-X-100 for 10 minutes, and rinse with PBS for 3 times afterwards, then block coverslips for 15 minutes with blocking buffer, which is PBST (0.1% Tween-20) containing 1% donkey serum. For stress granule visualization, incubate coverslips with primary antibody, goat-anti-eIF3η (dilute 1:100), for 1 hour. Wash coverslips with PBST for 3 times, each time lasts for 5 minutes, and then apply secondary antibody, goat-anti-Cy5, for 30 minutes. Wash 3 more times with PBST, and stain coverslips with 1μM DAPI for 1 minute. Rinse away the stain with PBS, then mount coverslips with Prolong-Gold mounting medium. Dry the coverslips in dark overnight, and acquire images by using DeltaVision Elite Microscopy with 60x objective. Every experiment was performed at least 3 times independently and quantified from 5-10 fields of images by using SoftWoRx.

Solubility test

Constructs were transformed into (which bacteria strain?), and one colony was cultured in 2 mL Luria Broth supplemented with 0.1 mg/mL ampicillin at 37 °C for 3 hours on the next day. Protein expression was induced by 0.5 mM IPTG at 37°C for 2 hours. Take 500 μL bacteria culture and spin down at maximum speed (14800 rpm) in a microcentrifuge for 1 minute. Decant supernatant and lysed cells with 100 μL lysis buffer [25 mM HEPES (pH=8.0), 500 mM NaCl, 20 mM β-mercaptoethanol, 10% glycerol, 1 mg/mL lysozyme, and 1x SigmaFast Protease inhibitor]. Freeze-and-thaw cycles was used for cell lysis, where samples were frozen immediately by liquid nitrogen, and

thawed in warm water with vortex. The cycles were continued thrice. Spin down lysed culture at aforementioned maximum speed at 4°C for 10 minutes, and take 30 mL supernatant as soluble part. For the insoluble part, pellets were resuspended with 100 μL water and 30 μL were taken for Western blot. Both soluble and insoluble samples were supplemented with SDS buffer and boiled at 95°C for 7 minutes with vortex occasionally. Proteins were probed by anti-FLAG and the ratio of protein expression in supernatant and pellet were compared to determine solubility.

Protein purification

Transform constructs by DE3-strain C41 competent cells, and grow transformed colonies in 1.5 L Luria Broth containing 0.03 mg/mL ampicillin at 37 °C till optical density reaches 0.5-0.6. Cool down the culture at cold room for 30 minutes, and induce protein expression by 0.3 mM IPTG at 16 °C for 16-18 hours. On the next day, spin down the culture at 5000 rpm for 15 minutes. Resuspend cells with 25 mL binding buffer (25 mM HEPES (For RNF-146 and PARP-13, pH=8.0; for GST, pH=7.0), 300 mM NaCl, 10 mM β-mercaptoethanol, 20 mM imidazole (pH 7.4), 10% glycerol, and 1x SigmaFast Protease inhibitor tablet and lyse by sonication (Amplitude 55%, 1.5 second on/ 4.5 second pulse, for 3 minutes). Centrifuge lysed cells at 12000 rpm for 30 minutes, and at the same time, equilibrate 5 mL HiTrap TALON crude FF column by 10 column volumes of binding buffer. Supernatant was applied to TALON column, washed with 10 column volumes of binding buffer, and eluted with binding buffer containing 250 mM imidazole. Eluted proteins were desalted by 5 mL HiTrap Desalting column in binding buffer. In order to get tag-free protein, cleavage was performed by 6x His-SENP protease

application (substrate: enzyme = 50:1) at room temperature for 1 hour. Cleaved protein products were further purified by reverse IMAC on 1 mL HisTrap crude FF column and gel filtration chromatography on HiLoad 16/600 Superdex 200 pg column in gel filtration buffer (20 mM Tris (pH 7.0), 200 mM NaCl, 10 mM β-mercaptoethanol, 5% glycerol). Proteins aliquots were frozen immediately by liquid nitrogen and store in -80 ˚C. Purity of proteins was analyzed by Coommassie blue staining, and probed by anti-FLAG and anti-His antibodies to identify size of proteins as well as SENP cleavage efficiency on western blot SDS-PAGE.

Slot blot assay

Concentration of purified proteins were measured by Nanodrop, and diluted to 10 pmol, 50 pmol, and 100 pmol in 10 μL gel filtration buffer. Rinse nitrocellulose membrane and 6 pieces of filter papers with TBS, and then assemble filter papers below membrane on Bio-Dot apparatus, remove residual buffer by 5 minutes of vacuum. Wash each well on the apparatus that were planned for sample loading with 200 μL TBS for 5 minutes. Mix protein samples with 40 μL gel filtration buffer, then load into wells, and vacuum for 5 minutes to confirm that all samples were moved down immediately toward the bottom of the apparatus and attached on the membrane. Wash each well with 100 μL TBS for 3 times, each wash lasts for 5 minutes. Dry the membrane at 65ºC for 20 minutes, and rinse once with TBST (0.15% Tween-20) slightly. Incubate membrane with 0.1 μM synthesized bulk PAR (from our collaborator [59]) at cold room overnight. On the next day, rinse the membrane with TBST, and determine total protein level by REVERT total protein stain kit (LI COR Biosciences) at 700 nm channel by Odyssey.

Block the membrane with 4% skim milk in TBST for 30 minutes and wash the membrane with TBST for 5 minutes once. Membrane was probed with primary antibody, rabbit-anti-PAR (Trevigen, 1:1000), for 1 hour, and then washed with TBST for 3 times. Secondary antibody, goat anti-rabbit IRDye 800 (1:20000) was applied for 30 minutes. Wash membrane 3 more times with TBST, and scan images by Odyssey.

1,6-hexanediol treatment

Pre-sterilized coverslips were coated with Poly-D-lysine (1:100 dilution in PBS) for 10 minutes. Wash twice with PBS and seed $3x10^5$ HeLa cells on coverslips in a 6-well plate. On the next day, transfect seeded cells with 2.5 μg plasmids of choice by Lipofectamin-2000 for 18-24 hours. Stress was induced by 500 μM sodium arsenite in complete DMEM for 60 minutes, then replace medium containing 500 μM sodium arsenite supplemented with or without 6% 1,6-hexanediol in complete DMEM for 5 minutes. Cells were fixed with 4% paraformaldehyde for 15 minutes and stain with eIF3η as described above in the "Immunofluorescence" section. Images were acquired using DeltaVision Elite Microscope.

Quantification and statistical analysis

Analyze immunofluorescence images of stress granules by SoftWoRx. Process of quantification is briefly described as below: select FITC channel, and use "2D-polygon" to mark all possible areas of stress granules. Adjust channel threshold to exclude background or interfering signals. Make sure that the selection differentiate objects one by one so that we could get the number of stress granule accurately. Next, use the "3D-

polygon" function to measure granule area in each z-section. The function allows us to sum up all sections together automatically, then we could define stress granule volume. Additionally, stress granule numbers could be analyzed simultaneously. For nucleus volume measurement, choose DAPI channel, and use "2D-polygon" to mark nucleus area. Fine-tuned the channel threshold to include the whole nucleus inside, and then use the "3D-polygon" function to dissect nucleus area of every z-sections. Sum up all sections together by SoftWoRx and we could acquire nucleus volume. In this study, mean volume represents the average volume of stress granules generated per cell, while total volume mentions the sum of the volume of stress granules produced by individual cell. Each measurement was analyzed per cell, and mean value was set by average all measurements in the group. Statistical analysis was performed using JMP 12 and Student's t-test was used for the whole study. Prism 6 or Excel was used to depict histogram and box plot.

Chapter III

Results

WWE domain is important for PARP-13 to co-localize with stress granules

PARP-13 localizes to stress granules during stress condition [55], but which protein domain of PARP-13 is required for such localization remains unclear. To identify the localization, we cloned different truncated forms of PARP-13 with EGFP tags at the N-terminus, transfected them to HeLa (K) cells and examined their localization by immunofluorescence after 30 minute treatment of 250 μM sodium arsenite. These constructs include PARP-13.1 and its splice variant, PARP-13.2, which lacks the PARP-like domain, truncation mutants insert 5 (residues 380-902), insert 8 (residues 380-698) and WWE domain alone (residues 594-699) (Fig. 1a). The co-localization of the expressed PARP-13 fragments and stress granules were measured by overlay of green (EGFP) and red channels (as stained with stress granule marker, eIF3η). Results of immunofluorescence indicate that approximately 90% of cells transfected with PARP-13.2 have been co-localizes with stress granules (Fig. 1b). In comparison, only 30% of PARP-13.1 transfected cells co-localizes with stress granules, indicating that the PARP-like domain somehow serves as an inhibitory role. Meanwhile, insert 5 and insert 8 shows similar patterns as the full-length constructs (Fig. 1b), suggesting that the N-terminus of PARP-13, which encompasses four RNA-binding zinc finger domains, are not making critical contribution for co-localization. Surprisingly, we have found 47% of cells expressing WWE domain alone, which is the putative PAR-binding domain, is also able to co-localize with stress granule (Fig. 1b). We have observed that the stress granule co-localization of insert 8, which contains an additional zinc-finger domain, is always

stronger than WWE domain alone. In order to exclude the co-localization of WWE domain with stress granules was caused by EGFP-tag, we have also checked how GFP co-localize with stress granules (Fig. 1b). The result shown that 20% of GFP transfected cells contributes to stress granule co-localization, which is lower than the WWE domain alone, indicating that additional factor besides GFP-tag are responsible for stress granule localization. Taken together, these data suggested the importance of WWE domain for PARP-13 to co-localize with stress granules.

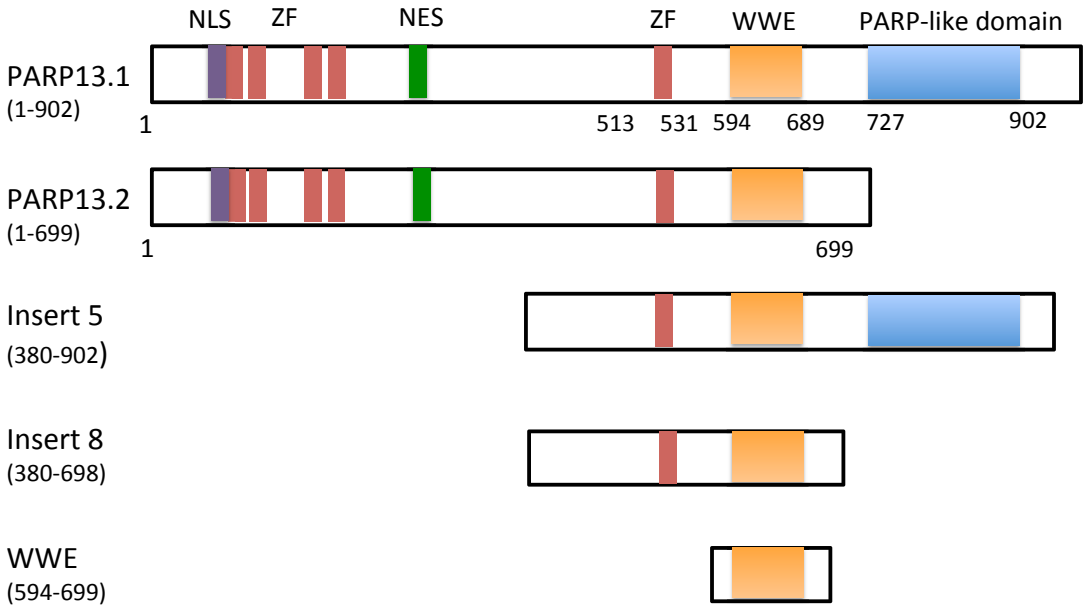

Figure 1a. Truncated forms of PARP-13 constructs.

Two isoforms of PARP-13 were used, PARP-13.1 (residues 1-902), which lack the PARP-like domain, and PARP-13.2 (residues 1-699). Insert 5 (residue 380-902) and insert 8 (residue 380-698), are truncated mutants of PARP-13.1 and PARP-13.2. The

WWE construct (residue 594-699) contains WWE domain only. References were taken from UniProt and NCBI websites.

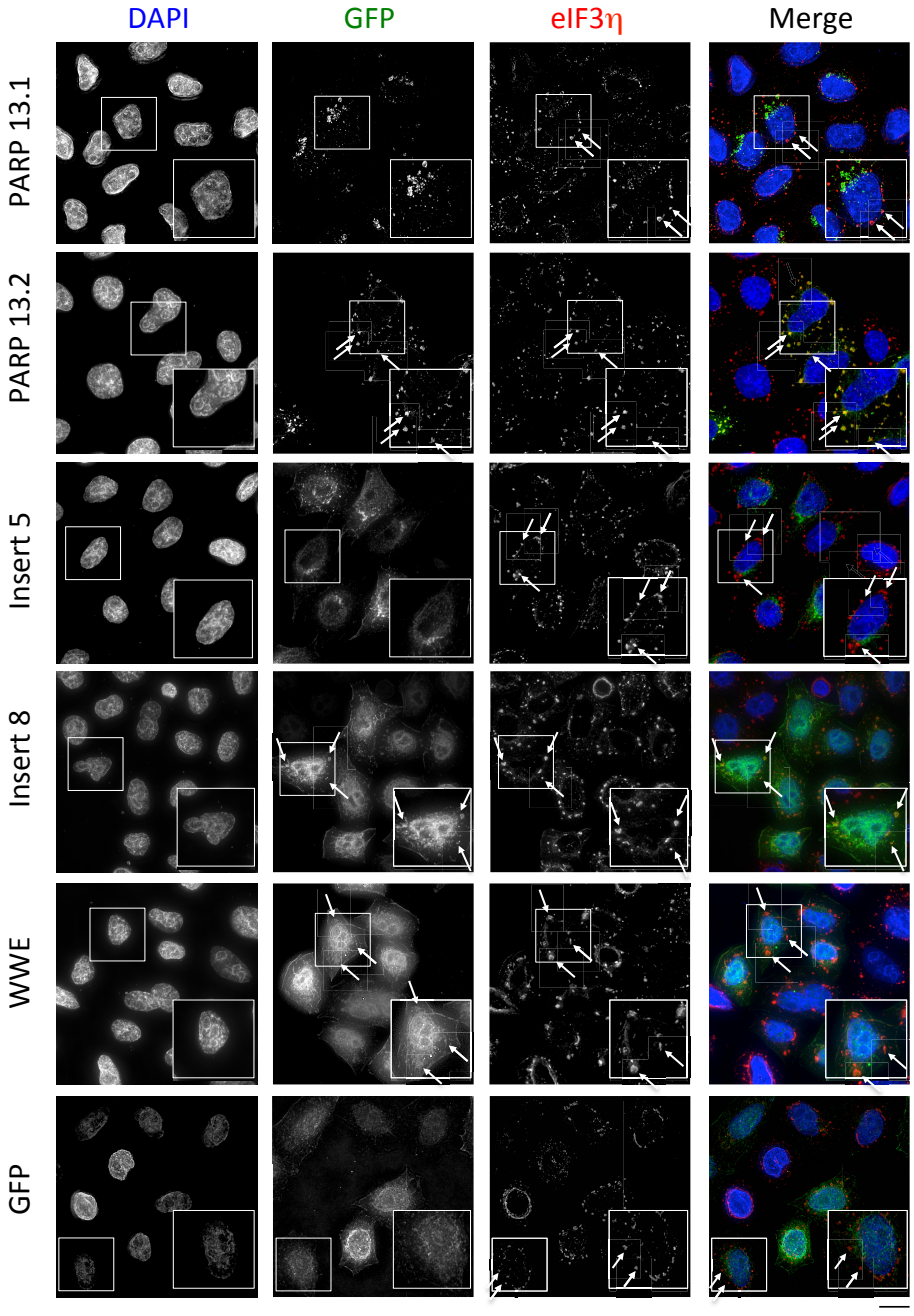

Figure 1b. WWE domain is important for PARP-13.2 to co-localize with stress granules.

HeLa(K) cells were seeded on coverslips for 24 hours, then transfected with 2.5 μg EGFP-tagged PARP-13.1, PARP-13.2, insert 5, insert 8, WWE, and GFP. Cells were stressed with 250 μM sodium arsenite for 30 minutes and were stained with anti-eIF3η to identify localization of stress granules. Scale bar: 10 μm.

Y659A on WWE domain contributes to smaller stress granules than PARP-13.2, while Q668A has intermediate size and numbers of stress granules

As PARP-13.2 co-localizes with stress granules and WWE domain seems critical for the co-localization, we next investigated how the domain regulates stress granules. Based on the sequence alignment of several WWE domains, including human RNF-146 and *Drosophila* Deltex, it is observed that Y659 and Q668 of PARP-13 are conserved with Y144 and Q153 of RNF-146 (Fig. 2a).

```
RNF146-WWE      ----------------------KAASRGNGEYAWYYE--GR-NGWWQYDERT--------
deltex          SEAETAGSGLLTIGVRRMFYAPSSPAGKGTKWEWSGGSADSNNDWRPYNMHV--------
PARP11-WWE      ------------------------MDTSDTQWGWFYL--AECGKWHMFQPDT--NSQCSV
PARP12-WWE2     --------------------------ILTTDWIWYWS--DEFGSWQEYGRQGTVHPVTTV
PARP13-WWE      -----------------------------KWIWYWK--NESGTWIQYGEEKDKRKNSNV
                                            .:  *        .  *   :

RNF146-WWE      -SRELEDAFSKG--------KKNTEMLIAGFLYVADLENMVQYRRNEHGRRRKIKRDIID
deltex          -QSIIEDAWAR------GEQTLDLSNTHIGLPYTINFSNLTQLRQPS-GPMRSIRRTQQA
PARP11-WWE      SSEDIEKSFKT-------NPCGSISFTTSKFSYKIDFAEMKQMNLTT-GKQRLIKR----
PARP12-WWE2     SSSDVEKAYLAYCTPGSDGQAATLKFQAGKHNYELDFKAFVQKNLVY-GTTKKVCR----
PARP13-WWE      DSSYLESLYQ-SCP------RGVVPFQAGSRNYELSFQGMIQTNIAS-KTQKDVIRRPTF
                 .  :*. :                        *  .:  : * .       : : *
```

Figure 2a. Highly conserved amino acid residues of WWE domains among RNF-146 and PARP-13.

Sequence alignment of different WWE domains indicated that in addition to W (tryptophan),W(tryptophan), and E (glutamate) residues (marked by grey asterisk), there

are other amino acids are highly conserved among different WWE domains, which are indicated by red frames. Alignment was determined by using Clustal Omega.

Structural study of RNF-146 indicates that both amino acids are critical for the binding of *iso*-ADP-ribose—the molecular structure spanning consecutive ADP-ribose subunits of PAR [53]. Therefore, we next test if mutating these amino acids affect stress granule formation. We created Y659A and Q668A mutants by site-directed mutagenesis and then transfected to HeLa (K) cells to check stress granules formation under 100 μM sodium arsenite treatment for 0, 30, and 60 minutes by immunofluorescence. At 0 min, we have found that some stress granules were formed in all groups (Fig. 2b, 1st row). It is known that some RNA-binding proteins, such as TIA-1 and G3BP1, are able to self-aggregate and promote stress granule assembly [60], which might partly explain that all three constructs could form stress granules without stress. However, there were no differences in the size of stress granules of wild-type PARP-13.2, Y659A, and Q668A (Fig. 2b, 1st row). When cells were treated with 100 μM sodium arsenite for 30 minutes, stress granules were observed in nearly all cells in each condition (Fig. 2b, 2nd row). Interestingly, the size of stress granules in Y659A was much smaller than the wild-type, and stress granule number was significantly increased. For stress granules of cells expressing PARP-13 Q668A mutant, the size was slightly smaller than the wild-type, and stress granule numbers sat in between those of wild-type and Y659A (Fig. 2b, 2nd row).

Studies on stress granules have indicated that the stress granules grow with time by fusing with adjacent stress granules [22]. For instances, stress granule area increases about 20% from 30 to 60 minutes of sodium arsenite treatment in U2OS cells [22].

Concerning about whether the fragmented granules were resulted from insufficient time for stress granules to grow bigger, we extended sodium arsenite treatment from 30 to 60 minutes. Data of 60 minutes demonstrated a similar pattern as in 30 minutes (Fig. 2b, 2nd and 3rd rows). The mean volume of stress granules in 60 minutes did increase, but not significantly, implicating that the size of granules has already reached maxima in 30 minutes. Compared with HeLa cells transfected with GFP-tagged TIA-1, it is shown that stress granule numbers reach the peak after 30 minutes of arsenite treatment. For stress granule size, the increment from 30 minutes to 60 minutes is approximately 10%, which were very similar as what we observed [24]. For quantification, we have used FITC channel to measure stress granule number and volume, and DAPI channel to analyze nucleus volume. The measurement we did here was a 3D analysis, which means that we calculated the granule volume instead of the granule area. In order to clarify the green channel represents stress granules, we have confirmed that every analyzed granules did co-localize with stress granule marker- eIF3η. Also, the threshold of each channel had been set appropriately that we can count different size of granules and exclude background signals. Based on these criteria, we have acquired more stress granules than described [61]. The possible reason for the difference was that we have analyzed 16 Z-sections by microscope (0.2 μm for each section), which might include more spatial fields than other studies [22]. Besides, we did not set a threshold to eliminate very small granules; instead to confirm the tiny dots are real stress granules, we have used co-localization with the stress granule markers eIF3η as an indicator. By quantification, stress granule numbers of Y659A is significantly more than the wild-type PARP-13.2 and the mean size is significantly smaller than PARP-13.2 during 30 or 60 minutes of arsenite

treatment (Fig. 2c). Comparatively, the pattern of stress granules of Q668A changes in a subtler, though statistically significant, manner. The stress granule number of Q668A is slightly more than PARP-13.2, and the mean volume is slightly smaller than PARP-13.2 (Fig. 2c). If grouping stress granules by size, the distribution of mean size is different among groups, where Y659A has more smaller stress granules, Q668A has intermediate ones, and PARP-13.2 has higher percentage of relatively larger stress granules (Fig. 2d). To examine whether wild-type and mutant WWE alter cell morphology, we have measured the volume of the nucleus at the same time. The results indicated that no significant difference of nuclear volume amongst PARP-13.2, Y659A, and Q668A, suggesting that transfection of different constructs did not affect basic physiological status (Fig. 2c). Before measuring the total volume of stress granules, we have assumed that the smaller stress granules of Y659A and Q668A from the previous immunofluorescence images might represent insufficient ability to form normal stress granules. If this is the case, the total volume of stress granules of the two mutants should be smaller than PARP-13.2. To our surprise, when we analyzed the total volume of stress granules, we did not observe any differences between groups (Fig. 2c), implicating that the wild-type PARP-13.2 and two mutants have similar ability to form stress granules. Smaller size of stress granules of the two mutants might be caused by losing supportive elements to hold each granule together; as a result, they cannot fuse together and form fragmented phenotypes.

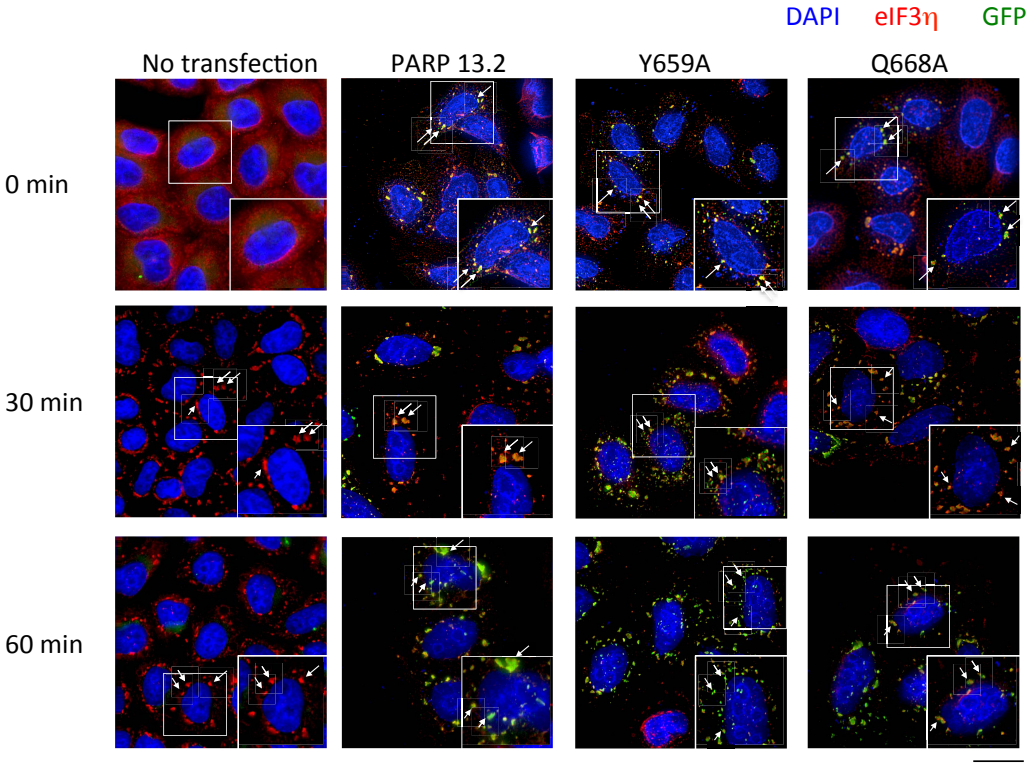

Figure 2b. Stress granules of Y659A mutant are more fragmented and smaller than PARP-13.2, while Q668A mutant has intermediate size and numbers of stress granules.

HeLa(K) cells were seeded on coverslips for 24 hours, then transfected with 2.5 μg EGFP-tagged PARP-13.2, Y659A, and Q668A. Cells were then stressed with 100 μM sodium arsenite for 30 or 60 minutes. Cells were stained with anti-eIF3η to identify localization of stress granules. Scale bar: 10 μm.

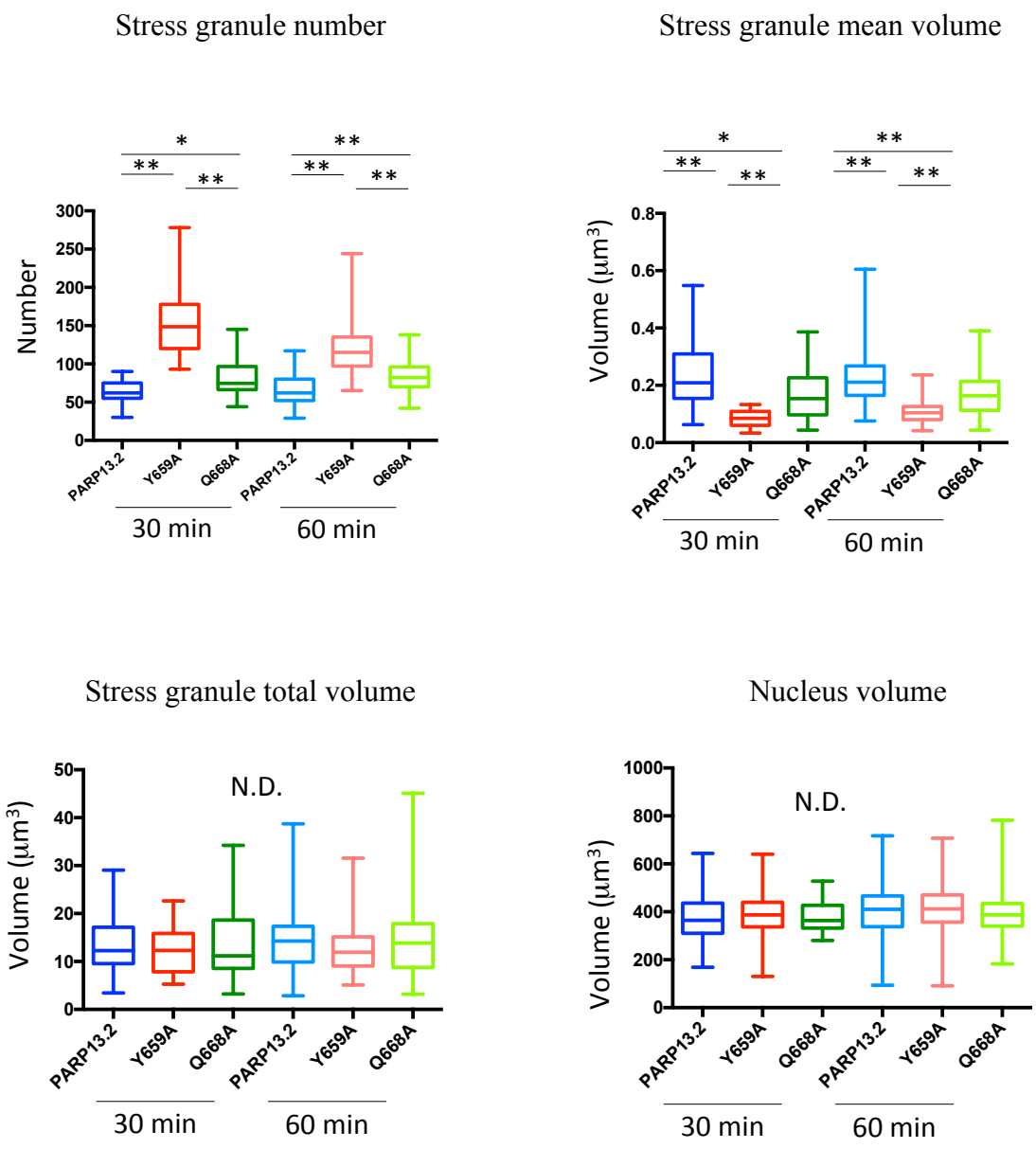

Figure 2c. Quantification data of stress granules of PARP-13.2, Y659A, and Q668A. Random fields were selected from 3 independent experiments. Utilize FITC channel to quantify stress granules by SoftWoRx. All parameters, including stress granule number, mean volume, total volume, and nucleus volume were measured by individual cell. Number of cells counted from each group was listed below: 30 minutes- PARP-13.2,

N=31; Y659A, N=30; Q668A, N=38, 60 minutes- PARP-13.2, N=95; Y659A, N=95; Q668A, N=98. JMP 12 was used to perform Student's T test. Single asterisk means p-value < 0.01, double asterisks shows p-value < 0.0001 as well. Scale bar: 10 μm.

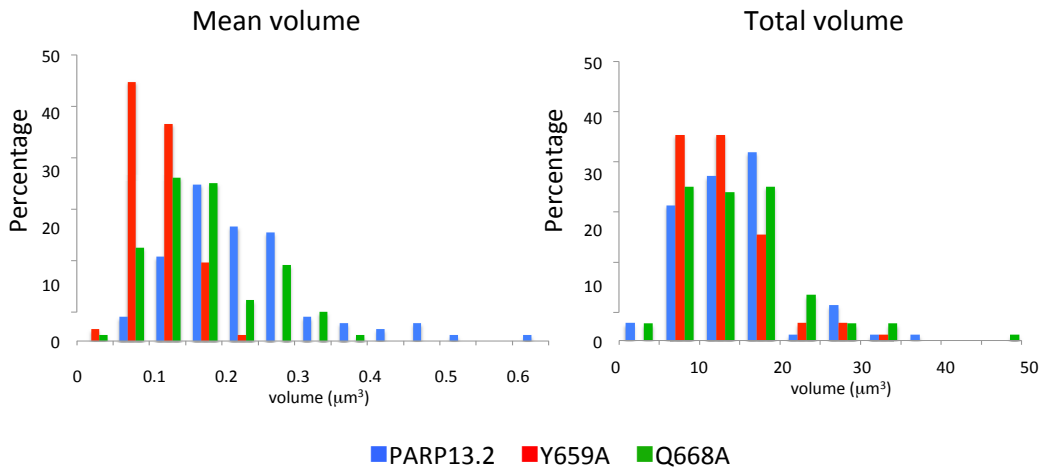

Figure 2d. Analyzing distribution of stress granules according to size.

Histogram depicts the distribution of stress granules according to size. Both mean volume and total volume of stress granules were analyzed.

Stress granule size in transfected HeLa (K) $^{PARP13-/-}$ cells share similar pattern as the wild-type HeLa (K) cells

To examine whether PARP-13 gene contributes to stress granule phenotype, and whether the same phenomenon of stress granules on Y659A and Q668A could be observed under PARP-13 knockout background, we have transfected EGFP-PARP-13.2,

Y659A, and Q668A to HeLa (K) $^{PARP13-/-}$ cell lines, and treated with 100 μM sodium arsenite for 0 or 30 minutes for immunofluorescence. We found that stress granules from transfected HeLa (K) $^{PARP13-/-}$ cell lines showed an identical pattern as in wild-type HeLa (K) (Fig. 2e). Stress granules could be induced slightly during 0 minute in all groups with similar size. During 30 minutes of sodium arsenite treatment, Y659A forms smaller size and fragmented stress granules, Q668A has intermediate size and number of stress granules, and PARP-13.2 possesses bigger size ones (Fig. 2e). The results indicated that mutation on Y659A and Q668A generate fragmented phenotypes of stress granules. Even though stress granules in HeLa (K) $^{PARP13-/-}$ cells are slightly smaller than wild-type HeLa (K), the difference is not significant. Quantification of stress granules of PARP-13 knockout cell lines has similar trend as the wild-type (Fig. 2f). The only difference is that the total volume of stress granules of PARP-13.2 is significantly bigger than Y659A and Q668A (Fig. 2f). If we compare the data of HeLa (K) wild-type and HeLa (K) $^{PARP13-/-}$ cells, the overexpressed PARP-13.2 groups demonstrated similar total stress granule volumes (Fig. 2c), indicating the addition of PARP-13.2 compensate for stress granule forming ability of knockout cells. The smaller total volume of Y659A and Q668A stress granules in HeLa (K) $^{PARP13-/-}$ cells indicated that the cells possess less ability to form stress granules compared to the wild-type HeLa (K) cells, implicating that PARP-13 is required for optimal stress granule formation.

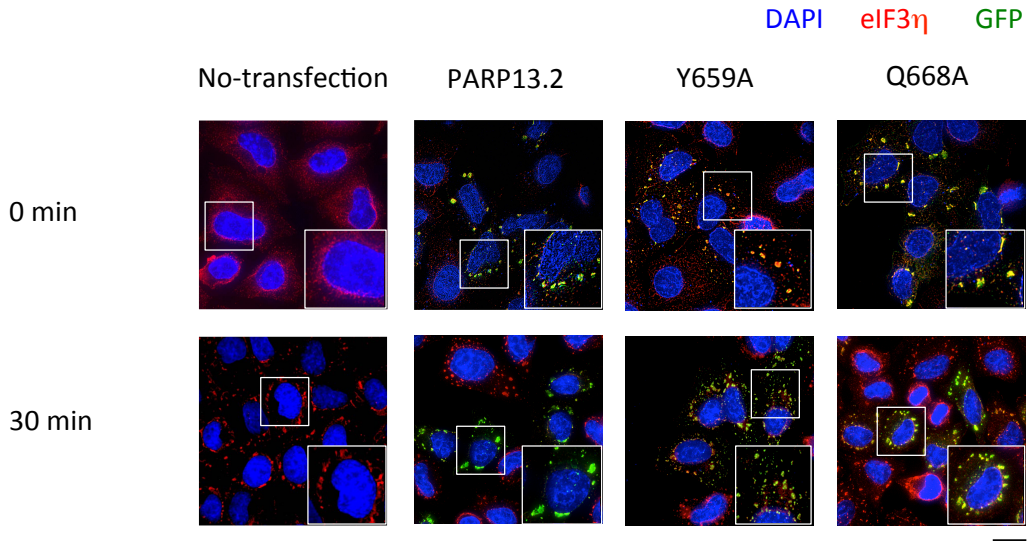

Figure 2e. Transient transfected EGFP-PARP13.2, Y659A, and Q668A in HeLa (K)$^{PARP13-/-}$ cell line shows similar stress granule patterns as in the wild-type HeLa (K) cells.

HeLa(K)$^{PARP13-/-}$ cells were seeded on coverslips for 24 hours, then transfected with 2.5 μg EGFP-tagged PARP-13.2, Y659A, and Q668A. Cells were stressed with 100 μM sodium arsenite for 30 or 60 minutes. Cells were stained with anti-eIF3η to identify localization of stress granules. Scale bar: 10 μm.

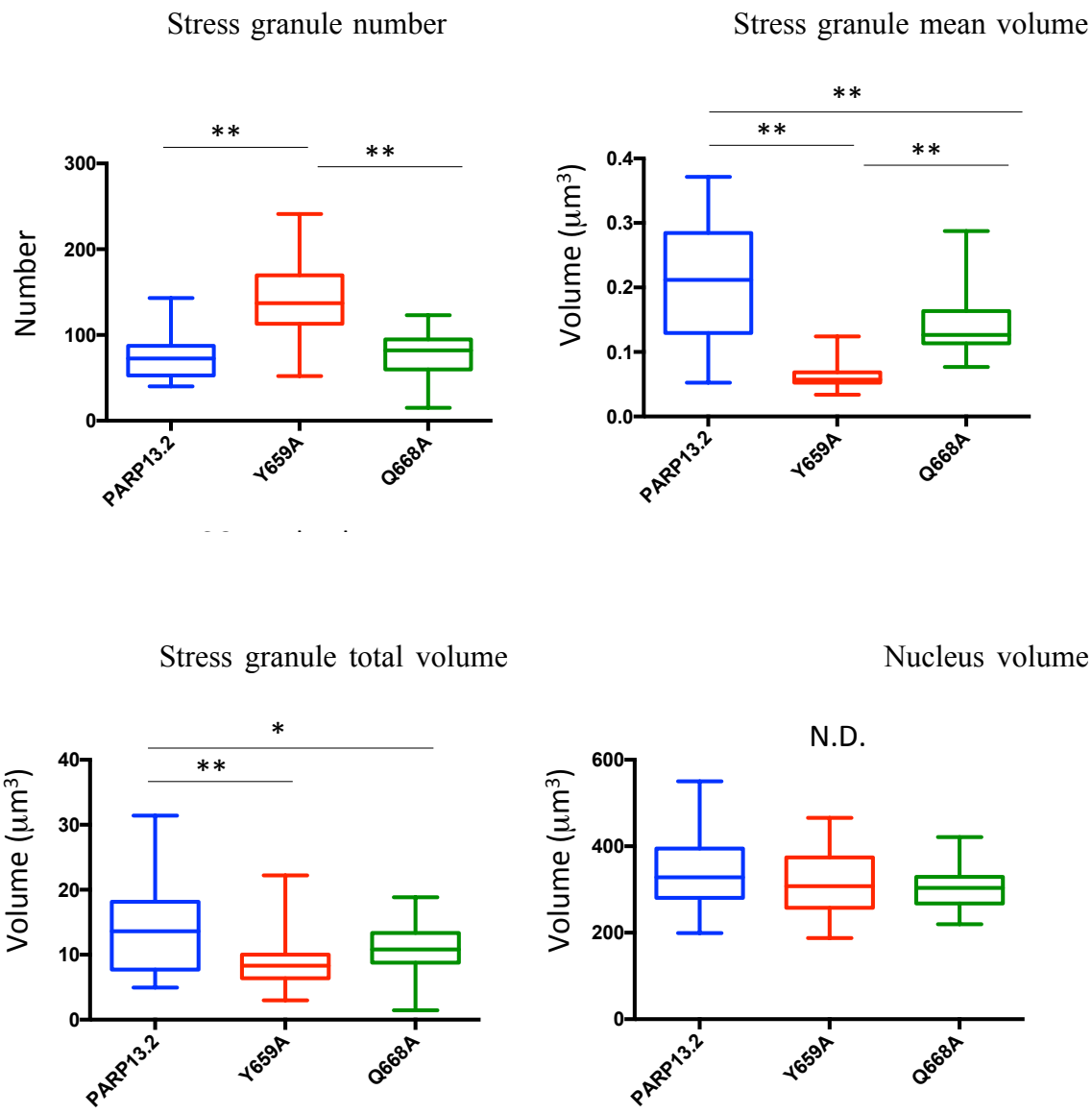

Figure 2f. Quantification data of transient transfected EGFP-PARP13.2, Y659A, and Q668A in HeLa (K)$^{PARP13-/-}$ cell line.

Random fields were selected from 2 independent experiments to quantify stress granules. Number of cells analyzed was listed below: 30 minutes- PARP-13.2, N=38; Y659A, N=25; Q668A, N=34. JMP 12 was used to perform Student's T test. Single asterisk means p-value < 0.01, while double asterisks shows p-value < 0.0001. Scale bar: 10 µm.

Similar fragmented stress granule pattern of Y659A and Q668A is observed in U2OS cells

Next, we tested whether the above stress granule phenomenon can be observed in other cell lines besides HeLa. Here we chose U2OS, human bone osteosarcoma epithelial cells, which is of distinct tissue origin from the human cervical HeLa cells. We transfected EGFP-PARP13.2, Y659A, and Q668A to U2OS cells, and treated them with 100 μM or 500 μM sodium arsenite for 0, 30, and 60 minutes to check stress granule by immunofluorescence. The pattern of stress granules in U2OS cells and HeLa (K) cells was very similar. Compared to the wild-type PARP-13.2, smaller and scattered stress granules was observed for Y659A and intermediate size and number of stress granules for Q668A during stress condition (Fig. 3). The only difference is that U2OS cells require a higher concentration or longer treatment of sodium arsenite to form stress granules. If we compare non-transfected cells between HeLa (K) and U2OS cells, the percentage of stress granules induced is different under same stress condition. For HeLa (K) cells, 100 μM sodium arsenite treatment for 30 minutes induced 80% cells with stress granules (Fig. 2b), while we hardly observed stress granules in U2OS cells under the same condition (Fig. 3). Taken together, the stress granule phenotypes of Y659A and Q668A are not only limited to HeLa (K) cells, but also in U2OS cells.

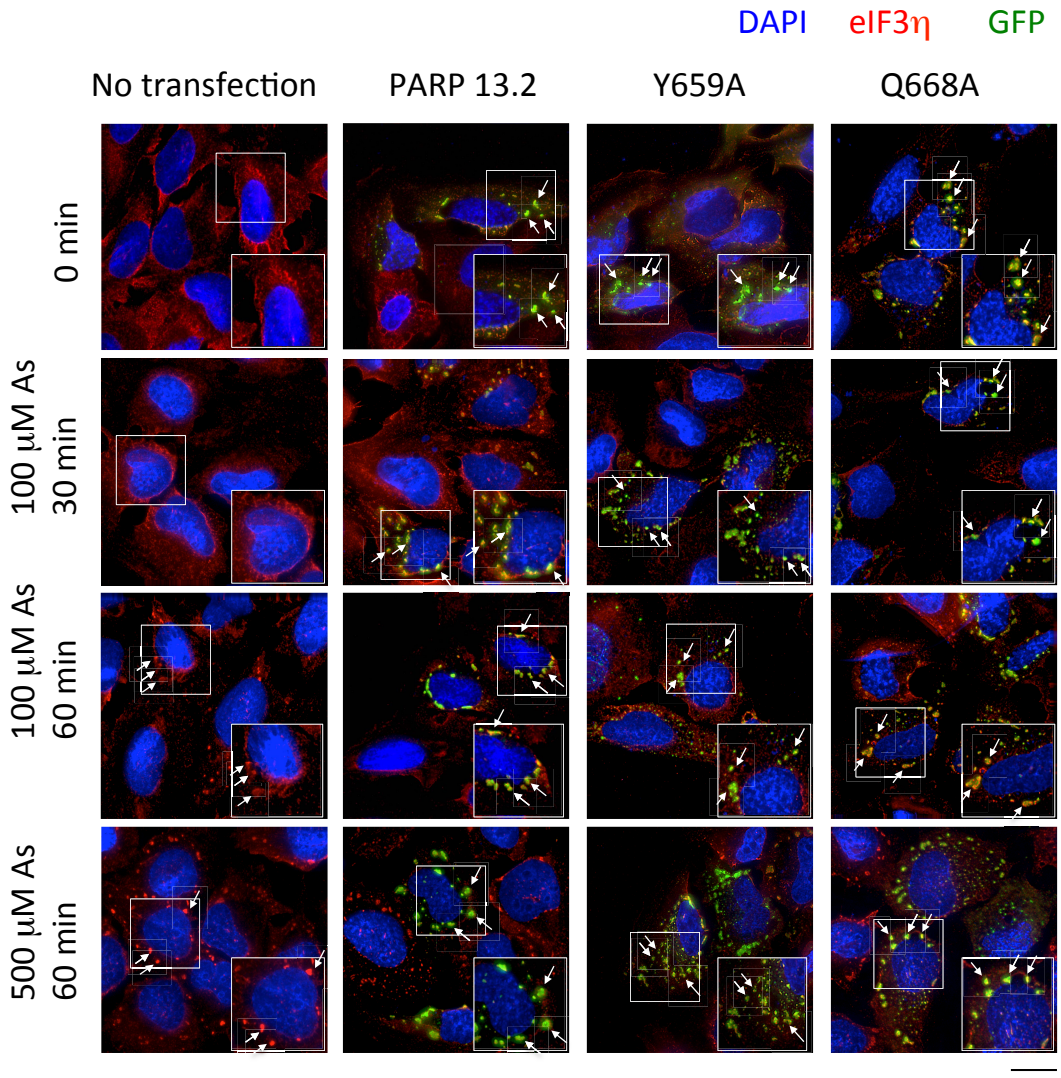

Figure 3. Similar stress granule patterns are also observed in U2OS cell line.

U2OS cells were seeded on coverslips for 24 hours, then transfected with 2.5 μg EGFP-tagged PARP-13.2, Y659A, and Q668A. Cells were stressed with 100 μM or 500 μM sodium arsenite for 30 or 60 minutes. Cells were stained with anti-eIF3η to identify localization of stress granules. Scale bar: 10 μm.

Purification of soluble PARP-13-WWE protein requires appropriate conditions

To evaluate the PAR binding ability of PARP-13-WWE, we were planning to use recombinant proteins for the *in vitro* PAR binding assay, including PARP-13-WWE-FLAG (594-689), RNF-146-WWE-FLAG (positive control), and GST-FLAG (negative control). However, we found that the PARP-13-WWE protein was insoluble during protein purification, which was also shown for the purification of Deltex WWE domain [62]. Different recipes of lysis buffer or detergents did not improve protein solubility. For lysis buffer containing urea [62], PARP-13-WWE formed severe precipitation during protein refolding, just as mentioned in ref. [53] that many WWE domains tend to form aggregation. After those trials, we decided to clone new constructs to solve insolubility. The cloning strategy was based on secondary structure prediction by JPred as well as conserved regions of N terminus and C terminus from sequence alignment analysis. We selected three promising sites from each terminus, and made different combinations for DNA cloning (Fig. 4a). After that, we have screened protein solubility, in parallel with the positive control RNF-146-WWE, by making small cultures of each construct and performing Western Blot. The results indicated that constructs BD (604-689) and BE (604-684) had the best protein expression on soluble part, even half of the proteins were still in the insoluble fraction (Fig. 4b). Thus, we decided to use BD construct for PARP-13-WWE protein purification.

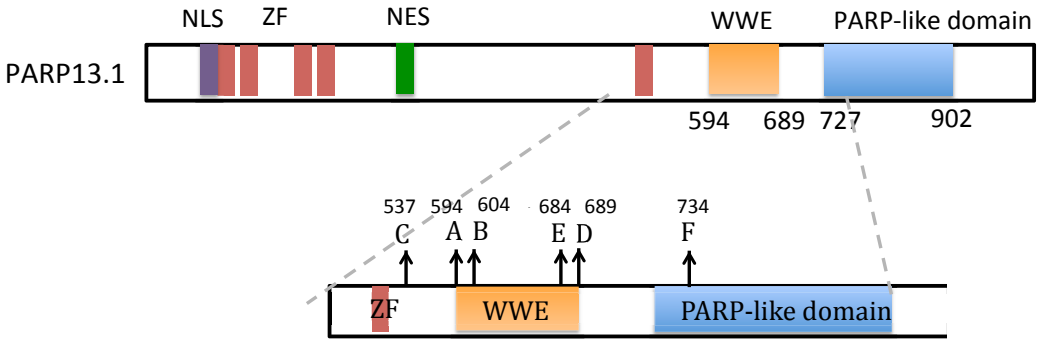

Figure 4a. Predicted sites for preparing pSAT1-PARP-13-WWE construct with stable structure.

Sequence alignment of WWE domain from different species has been done by using Clustal Omega. Also, JPred was used in parallel to check predicted secondary structures of those WWE domains. Then, three highly conserved regions were chosen from N terminus of WWE domain (A,B,C) and three from C terminus (D,E,F), to make different combinations (AD, AE, AF, BD, BE, BF, CE, and CF) for cloning stable PARP-13-WWE constructs.

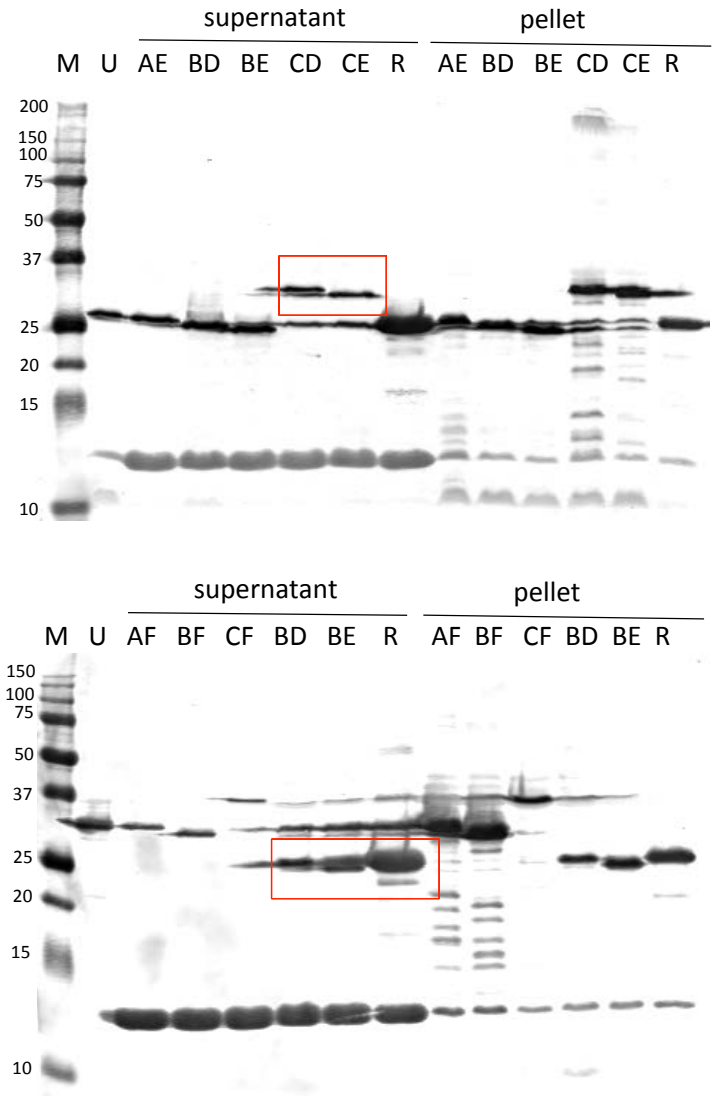

Figure 4b. Solubility test showed that BD (residues 604-689) and BE (residues 604-684), had the best soluble protein expression among all pSAT1-PARP13-WWE constructs.

Transformed constructs with DE3-C41 strain bacteria cells, and take one colony to make 2 mL luria broth culture. Protein expression was induced by 0.5 mM IPTG, and cells were lyzed by freeze-and-thaw cycles with vortex. Both supernatant and pellet were taken for Western blot and probed with anti-FLAG. Red frames indicated the bands of proteins according to expected size.

Proteins were expressed in DE3-strain C41 competent cells, cultured in Luira broth, and induced by 0.3 mM IPTG. Cells were lysed by sonication, and the soluble supernatant was taken for fast protein liquid chromatography (FPLC). From the chromatography results of TALON column, desalt column, and reverse IMAC column, we observed decent expression of proteins for these individual steps (Fig. 4c). At the last step, we separated protein peaks of PARP-13-WWE and His-SUMO-tag after SENP cleavage by gel filtration (Fig. 4c). To check the anticipated protein, we examined protein products from each purification step by Coomassie blue gel, and it showed that proteins got enriched after elution and His-SUMO tag was cleaved after SENP treatment (Fig. 4d, red frames). The protein at 36^{th} and 37^{th} fractions fit the expected size of PARP-13-WWE (~11 kDa), which were confirmed by anti-FLAG antibody (Fig. 4e). And the protein at the 50^{th} fraction has the same size of His-SUMO (~15 kDa), which was identified by anti-His antibody (Fig. 4f). However, from the 36^{th} and 37^{th} fractions, we also observed bands of higher molecular weight (~37 kDa) probed by FLAG antibody, which cannot be probed by His antibody, implicating those bands was not the full length His-SUMO-PARP-13-WWE-FLAG as a result of incomplete SENP cleavage. One of the possible reasons of the higher bands is that purified PARP-13-WWE tends to form aggregation, which requires future experiments to clarify. Therefore, we have obtained the purified PARP-13-WWE for PAR-binding assay.

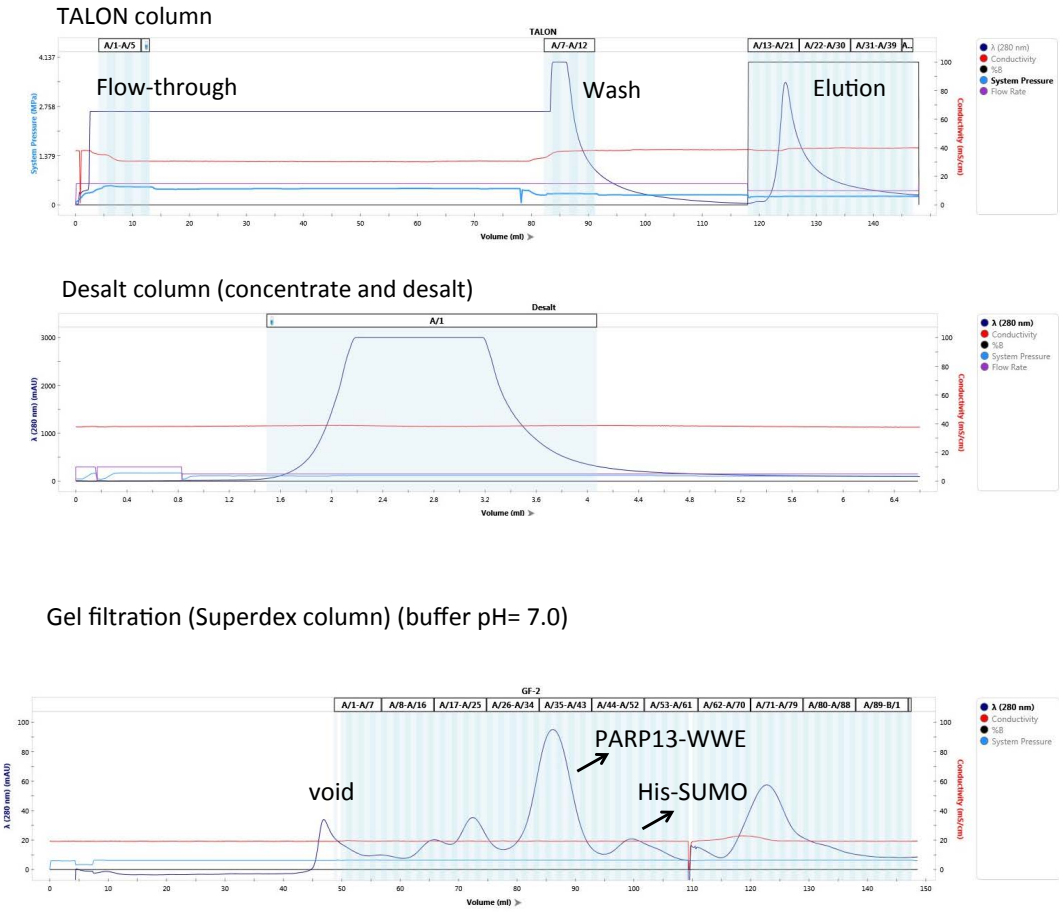

Figure 4c. Protein purification of PARP-13-WWE (604-689) using FPLC.

Fast protein liquid chromatography (FPLC) was used to purify PARP-13-WWE (604-689) protein. Construct was transformed with DE3-C41 strain bacteria cells, cultured in 6L luria broth, and induced by 0.3 mM IPTG at 16 ° C for 16-18 hours. Cells were lysed by sonication, and applied to TALON column and desalting column, and then treated with SENP. Reverse IMAC and gel filtration (Superdex 200 pg column) were further used to purify proteins.

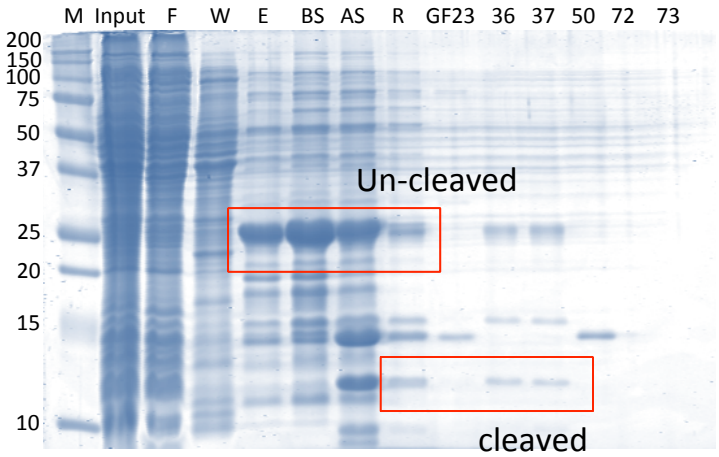

Figure 4d. Purity of PARP-13-WWE protein purification was examined by Coomassie blue staining.

Products from each purification step were taken to examine purity of proteins by Coomassie blue assay.

F: flow-through, W: wash, E: elution, BS: before SENP, AS: after SENP, R: Reverse IMAC, GF: gel-filtration (numbers represent which fractions were taken)

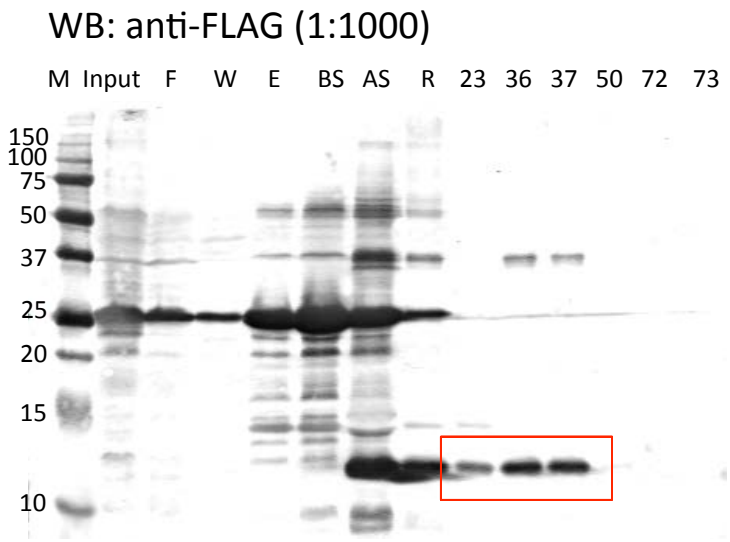

Figure 4e. PARP-13-WWE protein fractions from purification were examined by Western blot.

Products from each purification step were taken for Western blot and probed by anti-FLAG antibody .

F: flow-through, W: wash, E: elution, BS: before SENP, AS: after SENP, R: Reverse IMAC, GF: gel-filtration (numbers represent which fractions were taken)

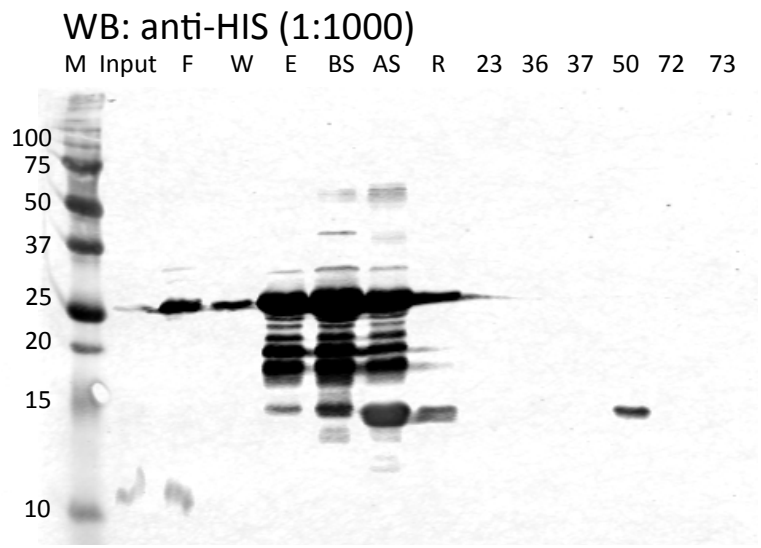

Figure 4f. PARP-13-WWE protein fractions from purification was examined by Western blot.

Products from each purification step were taken for Western blot and probed by anti-His antibody .

F: flow-through, W: wash, E: elution, BS: before SENP, AS: after SENP, R: Reverse IMAC, GF: gel-filtration (numbers represent which fractions were taken)

Recombinant PARP13-ZF-WWE protein is able to bind to PAR

In order to examine whether WWE domain of PARP-13 share PAR binding ability as RNF-146, we have performed dot blot assay by dotting 100 pmol of purified recombinant proteins of PARP-13-WWE (604-689), GST, and RNF-146-WWE on nitrocellulose membrane and incubating with 0.2 μM synthesize bulk PAR [59]. After washing, the membrane was blocked and probed with FLAG and PAR antibodies. The results indicated that RNF-146-WWE is able to bind to PAR *in vitro*, while GST is lacking of

the binding ability (Fig. 5a). For PARP-13-WWE, PAR signal could be observed. However, the signal was weak and not robust (Fig. 5a). We have assumed that one of the possible reasons is that the purified WWE domain was not stable and it lost binding ability over time. Recently, in collaboration with Dr. John Pascal (University of Montreal), we were able to obtain the purified PARP-13-ZF-WWE (residues 507-699) protein, which contains WWE domain and the fifth zinc finger. Therefore, we decided to use that protein to substitute our original one for PAR binding assay. In here, we have utilized slot blot assay to evaluate PAR binding ability. First, we loaded 10, 50, 100 pmol of each proteins on nitrocellulose membrane by Bio-Dot apparatus, then incubated the membrane with 0.1 μM bulk PAR. Total protein level was measured by total protein stain, which fluoresced at 700 nm, and the level of PAR was probed by anti-PAR primary antibody. Clear PAR signal was observed for PARP-13-ZF-WWE and RNF-146-WWE. For GST, we did not observe any PAR signal overlay with protein (Fig. 5b). To further check whether these proteins bind to PAR in a dose-dependent manner, equal amount of proteins were loaded on the nitrocellulose membrane: 50 pmol of GST, 100 pmol of RNF-146-WWE, and 10 pmol of PARP-13-ZF-WWE, and then incubated with 0.01, 0.05, and 0.1 μM of PAR *in vitro*. The results show again that both PARP-13-ZF-WWE and RNF-146-WWE binds to PAR, and the binding ability augmented when PAR concentration is increasing (Fig. 5c). Even though we did not have the mutant Y659A and Q668A proteins available for the test, which requires further investigation, we identified the PAR binding ability of the wild-type PARP13-ZF-WWE protein. Taken together, ZF-WWE domain of PARP-13 shares comparable PAR binding ability as the WWE domain

of RNF-146, though we cannot exclude the possibility that zinc-finger contributes to the binding (see Chapter V Future Direction).

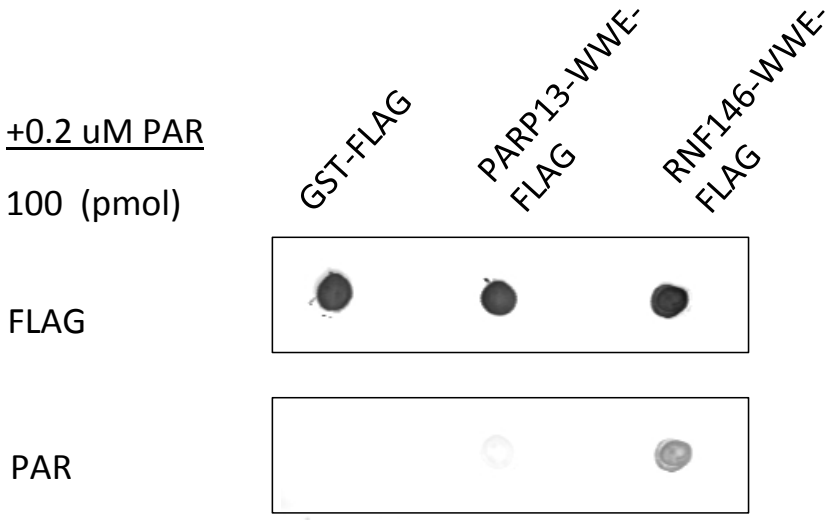

Figure 5a. Both WWE domains of RNF-146 and PARP-13 bind to PAR, but binding ability of PARP-13 is very weak and not stable.

100 pmol of purified proteins (2 μL) were dotted on nitrocellulose membrane, and the membrane was dried at 65 °C for 30 minutes. Next, the membrane was incubated with 0.2 μM bulk-synthesized PAR in TBST overnight. Membrane was then probed with anti-FLAG for total protein level and anti-PAR was used to measure PAR-binding ability of these proteins.

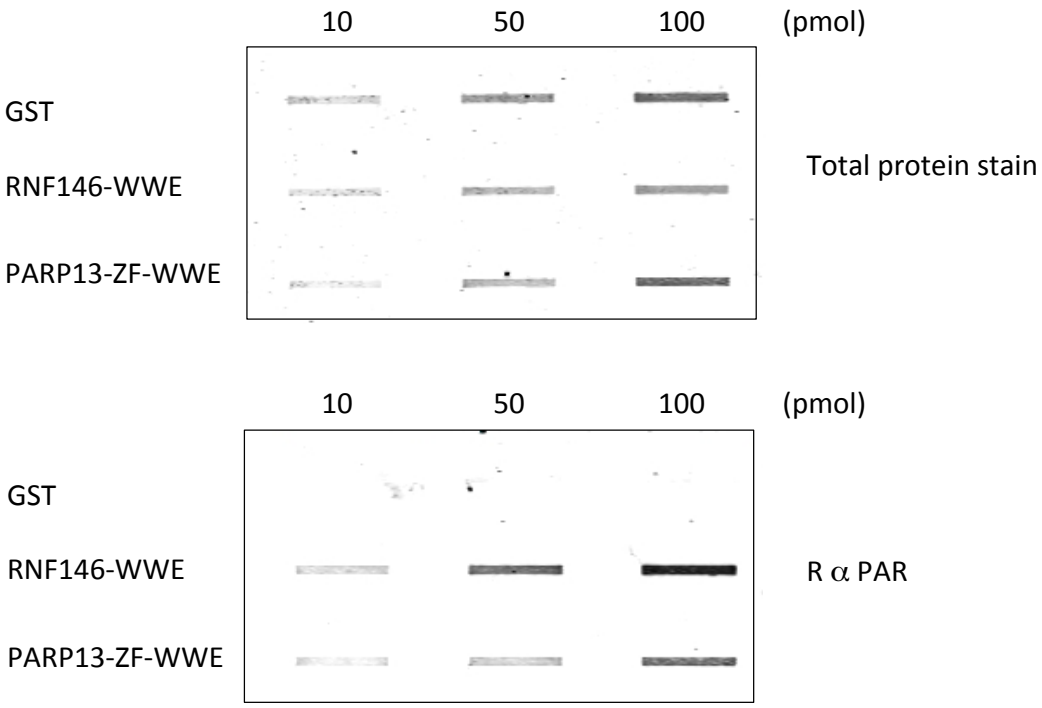

Figure 5b. WWE domain along with zinc-finger domain of PARP-13 is able to bind to PAR.

Different amount of purified recombinant proteins were used as indicated. 10 μL purified protein was loaded to wells of Bio-Dot apparatus. Each well was washed with 100 μL TBS, and then the membrane was incubated with 0.1 μM synthesized bulk PAR at cold room overnight. Total protein level was determined by REVERT total protein stain kit on the next day. Membrane was blocked and probed with anti-PAR (Trevigen, 1:1000) to measure PAR-binding ability. Images were acquired by Odyssey.

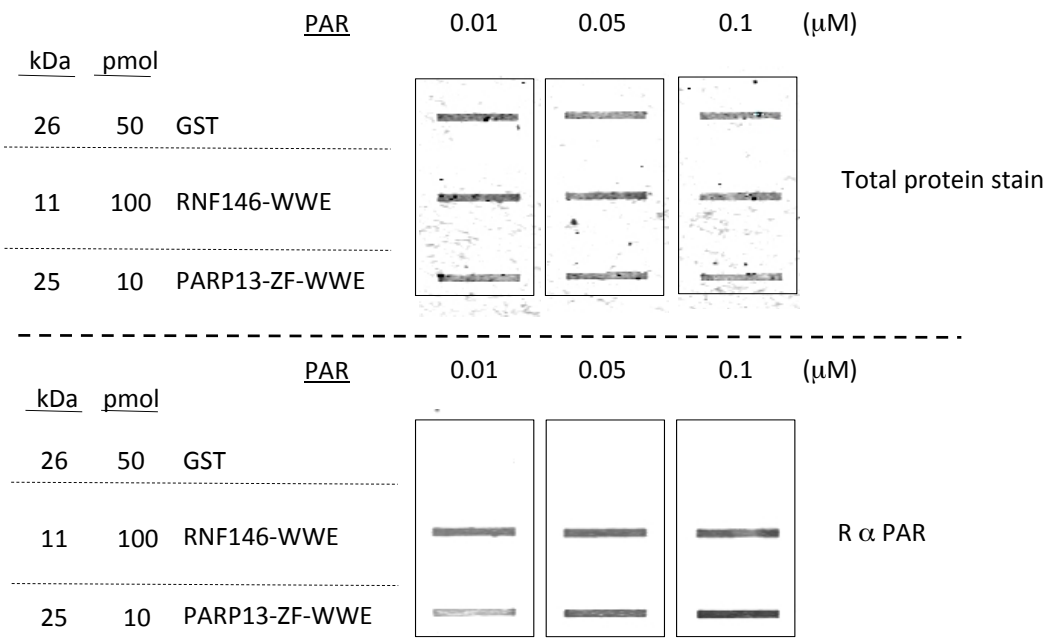

Figure 5c. Both WWE domain of RNF-146 and zinc-finger WWE domain of PARP-13 are able to bind to PAR in a dose-dependent way.

Equal amount of recombinant proteins were loaded to wells of Bio-Dot apparatus as indicated. Each well was washed with 100 μL TBS, and then the membrane was incubated with 0.01, 0.05, or 0.1 μM synthesized bulk PAR at cold room overnight. Total protein level was determined by REVERT total protein stain kit, and level of PAR was probed by anti-PAR (Trevigen, 1:1000). Images were acquired by Odyssey.

Stress granules of Y659A and Q668A are more resistant to 1,6-hexanediol treatment

In recent years, it is found that stress granules display features of liquid droplets, including fusion, shearing, and high dynamicity [22]. Studies have indicated that aberrant physical properties of granules could contribute to pathological process. For example,

polyglutamine (polyQ) aggregates, which has been connected to neurodegenerative disease, display a solid-like status while P-bodies and stress granules possess liquid-like feature [63]. Therefore, we next tested whether stress granules of PARP-13.2, Y659A, and Q668A have different physical properties. We transfected PARP-13.2, Y659A, and Q668A in HeLa (K) cells, and examined how stress granule dynamics are affected by using aliphatic alcohol, 1,6-hexanediol after stress [63]. The chemical could disrupt weak protein-protein or protein-RNA hydrophobic interactions and dissolve liquid-like structures instead of solid ones [10]. In addition to our original constructs, we have added one of the main stress granule proteins, G3BP1, as a comparison in this experiment. Immunofluorescence results indicated that over-expression of all proteins resulted in 30% of transfected cells forming stress granules without stress and the formation of stress granules were induced further under sodium arsenite treatment, which is similar as we described earlier (Fig. 6a, 1st and 2nd rows; see also Fig. 2b). For PARP-13.2, Y659A, and Q668A, the percentage of stress granules in stressed conditions was higher than Fig. 2b, which might be caused by treatment with a higher concentration of sodium arsenite. Treatment of 1,6-hexanediol seems toxic to cells because almost all cells become round even though the coverslips have been pre-treated with poly-D-lysine. The morphology of cells were also changed, such as the formation of bulges in the cytosol. For all four groups, existing stress granules got smaller after the 1,6-hexanediol treatment, and the remaining cells possess different percentages of stress granules. For G3BP1 and PARP-13.2, most stress granules were disappeared by 5 minutes of drug treatment; while Y659A and Q668A remained (Fig. 6a, 3rd row). We have quantified the percentage of stress granules in GFP positive cells, and the analysis demonstrated that G3BP1 and

PARP-13.2 transfected cells almost lost 50% of stress granules, while Y659A and Q668A transfected cells still have 90% of cells with stress granules (Fig. 6b). The remaining stress granules of PARP-13.2 and G3BP1 under 1,6-hexanediol treatment displayed reduced granule numbers. On average, all granules became smaller but remained in a comparatively bigger size, which might be the stable core structure mentioned by other groups [22]. For Y659A, the remaining stress granules under 1,6-hexanediol treatment possessed fragmented phenotype, and the shrinkage of cell make them look more crowded than arsenite treatment alone. For Q668A, the remaining stress granules were smaller and scattered by large, however, the extent of fragmentation was less than Y659A. The result indicated these stress granules of wild-type and mutant PARP-13.2 have different physical properties, implicating that the predicted PAR binding ability probably affect stress granules' dynamics, which requires additional analyses with multiple time points by live cell imaging for further investigation.

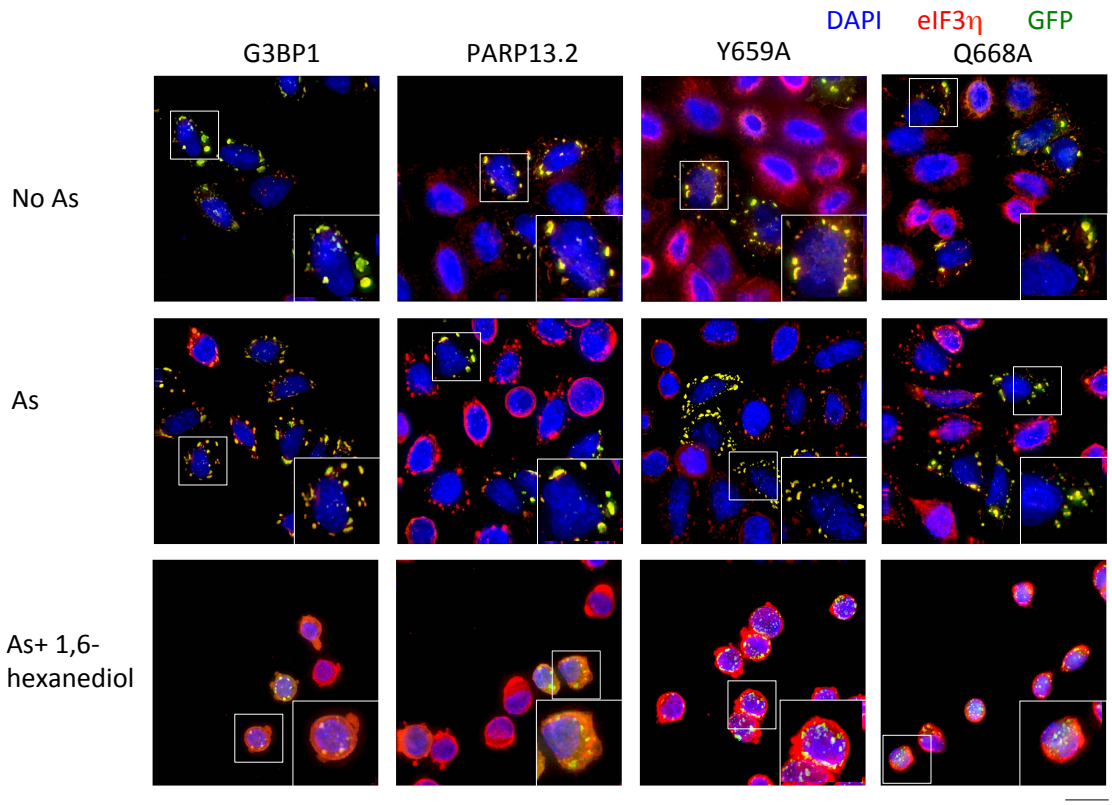

Figure 6a. Stress granules of Y659A and Q668A mutants are more resistant to 1,6-hexanediol treatment

HeLa(K) cells were seeded on coverslips for 24 hours, then transfected with 2.5 μg EGFP-tagged G3BP1, PARP-13.2, Y659A, and Q668A. Cells were stressed with 500 μM sodium arsenite for 60 minutes, then applying 6% 1,6-hexanediol for 5 minutes. Cells were stained with anti-eIF3η to identify stress granules. Scale bar: 25 μm.

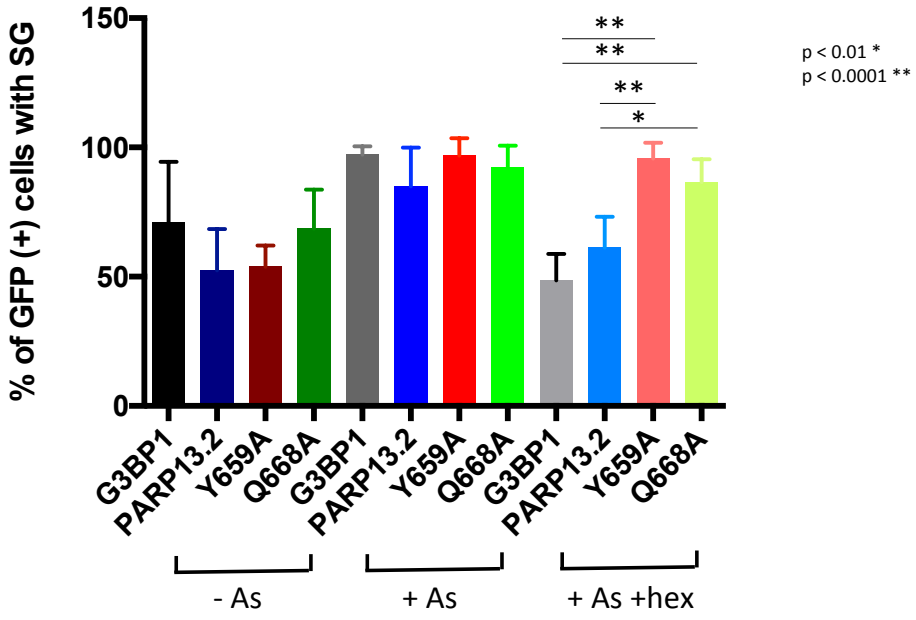

Figure 6b. Quantification data indicated that stress granules of Y659A and Q668A mutants are more resistant to 1,6-hexanediol treatment

Histogram shows quantification of percentage of GFP positive cells with stress granules after 1,6-hexanediol treatment. The measurement is defined as number of cells containing GFP punctum divided by number of cells containing GFP signals. Each bar represents mean value of each group from 4-7 independent experiments.

Chapter IV

Discussions

From previous studies, we have learned that PARP-13 is able to co-localize with stress granules under arsenite treatment, even though the required domains for co-localization remain unclear. In Fig. 1b, we found that two isoforms of PARP-13 display different percentage of stress granule co-localization. For PARP-13.1, it is found that only 30% of co-localization, while PARP-13.2 has 90% of co-localization. Under stress,

the modification of ADP-ribose is dramatically increased in PARP-13.2, but not PARP-13.1 [55], implicating that different level of modification might contribute to distinct co-localization. In addition, PARP-13.1 forms granules with distinct appearances that the fluorescent signals locate on the outer surface of the membrane. Moreover, those granules do not co-localize with stress granules, and some of them dock adjacent to stress granules instead. It is possible that the granules belong to other non-membranous structures, such as P-bodies, which requires further analyses. Studies have indicated that P-bodies usually dock with stress granules under stress, which might be related to regulate mRNA translation or degradation [2]. Other evidence indicated that PARP-13.1 was targeted to membranes by C-terminal CaaX motif [57], and the localization was mediated by farnesylation. The farnesylation on cysteine 899 enables PARP13.1 to localize to endoplasmic reticulum [64] while mutate the farnesylated site on cysteine 993 to serine residue redistributed PARP-13.1 to cytoplasm [65]. For insert 5 and insert 8, it is found that they have similar stress granule co-localization as their corresponding full-length proteins, PARP-13.1 and PARP-13.2 separately (Fig. 1b). These data suggest that the N-terminus of PARP-13, which contains four CCCH-type zinc fingers, is not necessarily required for stress granule co-localization (Fig. 1b). The deletion or mutation of the four zinc fingers reduced RNA-binding ability of PARP-13 [57], reflecting that the co-localization does not necessarily dependent on RNA-binding ability of these N-terminal zinc fingers. Even though PARP-12 shares high sequence homology as PARP-13 (Fig. 7), the domain requirement for stress granule co-localization is different. It is demonstrated that deletion of the first four zinc fingers or mutation of zinc finger on H208R will form punctate foci that are distinct from stress granules [66], which is not the case for the

truncated form of PARP-13−insert8. The most surprising part is that WWE domain alone is also able to co-localize with stress granules, even though the co-localization is always weaker (47%) than insert 8 (65%) (Fig. 1b). We can exclude unspecific signal background by differentiating co-localization of WWE domain from the negative control GFP (20%). It is, however, unclear whether the co-localization of insert 8 was contributed by the addition of the fifth zinc-finger on the N-terminus of this construct (Fig. 1a), to make the protein structure more stable or co-localize through RNA-binding. It requires future experiments to test if the fifth zinc finger possesses RNA-binding ability. Taken together, the WWE domain in PARP-13 potentially serves an important role for stress granule co-localization and we would like to further investigate its mechanism.

WWE domain has been characterized in specific proteins that mediate protein-protein interaction in ubiquitination and ADP-ribosylation [52]. The functions of WWE domains in ubiquitin-E3 ligase were better understood. One of the most well studied WWE domains in E3-ligase is RNF-146, which is able to bind to *iso*-ADP-ribose [53] and couple ubiquitination and PARylation [67]. Comparatively, functions of WWE domains in PARP family proteins were only identified in some PARPs. Structural studies of PARP-11 revealed that the WWE domain is able to recognize ADP-ribose, while the WWE module of PARP-14 barely recognize adenosine moiety [68]. For PARP-13, the structure and the function of WWE have not been clarified. In order to examine the putative PAR binding ability of PARP-13, we have selected amino acids by sequence alignment between RNF-146 and PARP-13, which might be crucial for ADP-ribose

binding ability, as our candidates for mutagenesis (Fig. 2a). Then, we performed site-directed mutation on those amino acids and checked how such changes affect stress granules. Interestingly, we identified new phenotypes of stress granules by only one amino acid mutation on WWE domain of PARP-13, Y659A and Q668A (Fig. 2b). The comparable total volume of stress granules in wild-type, Y659A and Q668A mutants demonstrated all share similar ability to form stress granules. These data suggest that the smaller and fragmented phenotype of stress granules might be resulted from defected fusion ability. Even though the overexpression of PARP-13.2, Y659A, and Q668A creates a small portion of stress granules under normal condition, there were no significant difference in the size and number of granules, implicating that the phenomenon of stress granules is stress-dependent (Fig. 2b). In addition, the fragmented pattern of stress granules was not restricted to HeLa (K) cells, but was also observed in HeLa $(K)^{PARP13-/-}$ (Fig. 2c) and U2OS cells (Fig. 3). For HeLa $(K)^{PARP13-/-}$ cells, we have observed that PARP-13 knockout does not affect stress granule formation under stress. The only difference is that the granules of knockout cells are slightly smaller than wild-type ones (Fig. 2b and 2c). In addition, it requires stronger stress stimulation to induce similar extent of stress granules, which implicates PARP-13 could enhance stress granule assembly. Given that PARP-12 has similar domain architecture and sequences (Fig. 7), PARP-12 and PARP-13 might play redundant roles in forming stress granules.

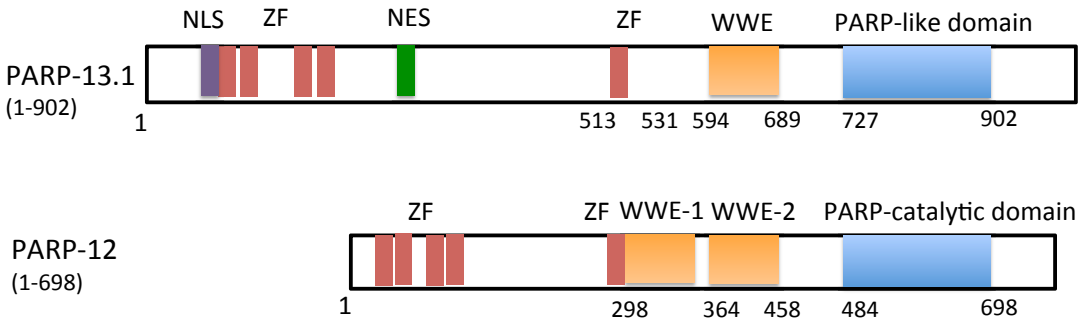

Figure 7. Domain architectures of PARP-12 and PARP-13

PARP-12 and PARP-13.1 share similarities on domain architectures. Domain information was taken from UniProt: PARP-12 (2PQF);PARP-13.1 (2X5Y).

Studies have indicated that knockdown of PARP-13 in HeLa cells decreases cell viability, suggesting that the smaller stress granules of HeLa (K)$^{PARP13-/-}$ cells might lose ability to sequester essential factors to maintain viability [54]. Transfected Y659A and Q668A to HeLa (K)$^{PARP13-/-}$ cells also display fragmented stress granules as in the wild-type HeLa (K) cells (Fig. 2c), demonstrating the supplementation of WWE mutants cannot compensate for the formation of stress granules with normal size. Instead, they remained fragmented. Without endogenous PARP-13, Y659A and Q668A in HeLa (K)$^{PARP13-/-}$ cells displayed similar mean volume but smaller total stress granule volume, suggesting that PARP-13 is a critical element for stress granule formation. For U2OS, which is of tissue origin different from HeLa (K), similar types of stress granules were observed. The observation of similar fragmented phenomenon of stress granules in different cell lines suggests that stress granule regulation by WWE domain is not restricted to specific cell type.

For the PAR binding assay, we have tried to purify PARP-13-WWE domain (594-689) first for *in vitro* binding assay. However, the expression of soluble protein was not ideal. Even though we have improved the solubility by choosing different DNA regions (604-689), the PAR binding is not robust (Fig. 5a). According to the latest analyses based on structural alignment on PARP-13 from our collaborator, it is identified that PARP-13 contains two WWE domains (Fig. 8). The first one is ranging from residue 534-589, which is located between the fifth zinc finger and the studied WWE domain, and the second one is from residue 607-686.

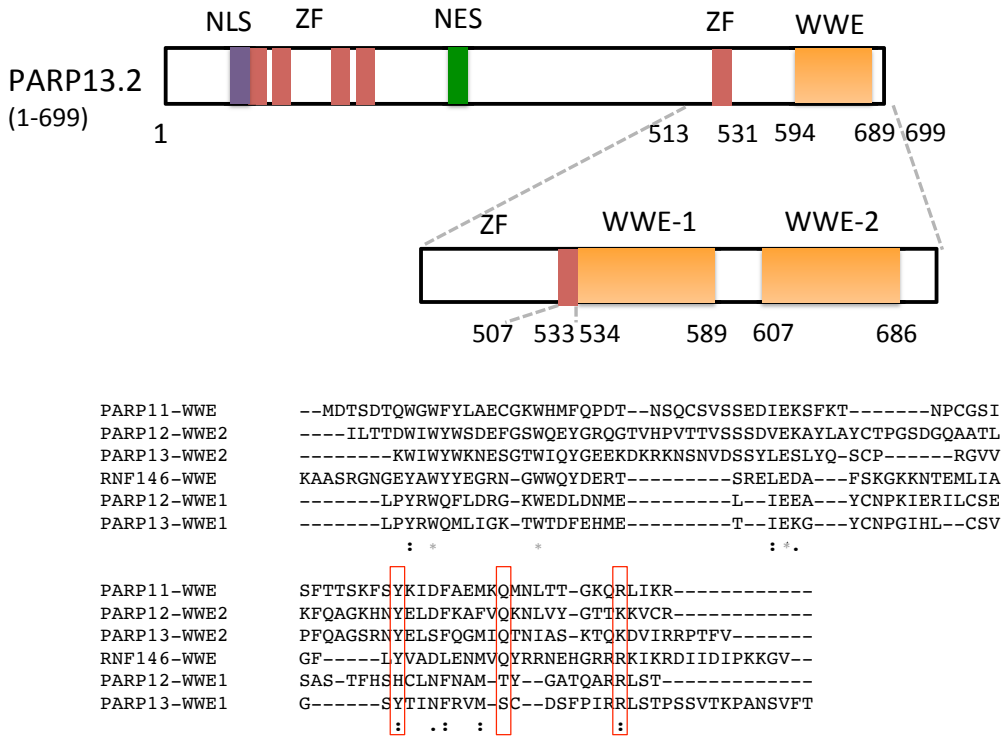

Figure 8. Proposed two WWE domains of PARP-13.

According to structural alignment analysis by our collaborator, Dr. John Pascal from University of Montreal, PARP-13 possess two WWE domains, which is similar as PARP-12. Sequence alignment was determined by using Clustal Omega. WWE domains were indicated by grey asterisk. The other highly conserved residues were marked by red frames.

Structural studies have indicated that Drosophila Deltex contains two tandem WWE domain repeats. The two domains folded similarly and coupled thermodynamically. Besides, the two modules interact extensively and forms a large cleft for substrate binding [62]. The two WWE domains of PARP-13 might work in the same way, therefore, it may be hard to purify them separately. Based on Fig. 5b and 5c, PARP-13-ZF-WWE binds to bulk PAR. The overlaid PAR signal is pretty clear, though we need more data with various concentrations of proteins/ligands to definitively calculate its affinity. At this moment, we are not sure about whether the binding affinity of PARP-13-ZF-WWE is comparable to RNF-146-WWE (*iso*-ADP-ribose $K_d = 0.37 \pm 0.02$ μM) [53]. Comparatively, the identified PAR-binding WWE domains of PARP family display weaker PAR binding ability. For example, PARP-11-WWE possesses weak binding ability to ADP-ribose ($K_d = 400 \pm 0.2$ μM), and PARP-14-WWE does not bind to PAR [68]. It is proposed that numerous WWE containing proteins are potentially cluster around PAR polymer [53], therefore, it requires more studies to investigate whether the two WWE domains of PARP-13 work cooperatively as Deltex1 [62] or display stronger binding to PAR.

The physical properties of RNA granules have been highly discussed in recent years. Evidence had shown that stress granules are formed via liquid-liquid phase separation that the liquid-droplets could fuse together or relax to spherical shape after shear stress [22]. Liquid-like properties allow components in stress granules to maintain high dynamics and facilitate its function [69]. The transition of liquid-like granules to solid-like ones is implicated as a detrimental process for causing neurological diseases [70]. In our study, it is found that granules of PARP-13.2 and G3BP1 dissolve within 5 minutes of 1,6-hexanediol treatment while Y659A and Q668A are more resistant to interruption of hydrophobic interaction (Fig. 6a). One interpretation could be that stress granule assembly of PARP-13.2 depends on PAR; therefore, breaking up the weak interactions, including PAR, disrupts and dissolves stress granules. On the other hand, stress granules of Y659A and Q668A were less dependent on PAR binding and the granules did not disassemble during 1,6-hexanediol treatment. Studies have shown that mRNA is able to impact on droplet properties, including phase separation, altering viscosity, and exchange rate of components with bulk solution [69]. Interestingly, different mRNA display distinct roles on biophysical properties, some will make granules more fluid-like and some will make them solid-like [69]. Many factors are involved in the regulation, such as protein/RNA ratio, RNA length, and RNA sequences [69]. In P granules, it is known that non-specific polyU RNA could fluidize droplets of protein LAF-1. Besides, RNA binding of polyQ proteins prevents or slows down protein transition to solid-like state [69]. Sharing similar repetitive and multivalent structures as RNA, it is possible that PAR is able to modulate biophysical properties of proteins. From our data, it suggests that the PAR-binding ability regulates dynamic of stress granules,

that PAR-binding makes the granules more soluble compared to those weak binder or non-binder. Studies of PARP-12 has revealed that the WWE domain was associated with ubiquitination on higher molecular weight, implicating the putative PAR binding domain might regulate ubiquitination and protein degradation by autophagy via ADP-ribosylation [66]. We cannot exclude the possibility that PAR-mediated ubiquitination also happens for PARP-13, which might be the reason for why granules of PARP-13.2 disassemble faster than Y659A ones. The change of protein physical properties by one amino acid mutation has been reported in Amyotrophic Lateral Sclerosis (ALS)-linked proteins. It is found that ALS-linked protein variant FUS- G156E, mutant on the PLD, tends to form aggregates and undergo liquid-to-solid phase transition. From the FRAP analysis, the mutant FUS converts to a solid-like fibrous state and cannot recover after eight hours [70]. Though the mechanism of transition is not well understood, the *in vitro* formation of protein crystals have been observed before phase transition [70]. It is proposed that saturated amount of proteins in liquid-phase trigger the nucleation of crystals, or the orientation of molecules at phase boundary are thermodynamically unstable that stimulate the crystallization [70]. Another theory is that the maintenance of liquid-like protein status required the input of energy to prevent the formation of aggregation. Thus, ATP-dependent protein chaperones and RNA-helicases were known to actively control the architecture as well as the composition in non-membranous organelle. Once the energy is out-of-equilibrium, then the intermolecular interactions might be disrupted and contribute to phase transition [71]. The phase transition could be stimulated by recruitment of misfolded proteins. A recent study has indicated that misfolded protein Ubc9TS co-assemble with stress granule protein-FUS and promote the transition of stress granules to

aberrant solid-like state [72]. Therefore, it is possible that mutations on WWE domain are inclined to recruit misfolded proteins to change properties of the granules.

Chapter V

Future directions

How does the fifth zinc finger contribute to stress granules?

Even though we have acquired promising data that ZF-WWE domain of PARP-13 binds to PAR, we are not sure about whether and, if so, how the fifth zinc finger contribute to the binding. Does it assist structure folding to maintain the stability of two WWE domains to facilitate stronger PAR binding, or does it contain RNA-binding ability, or even PAR-binding ability, for the formation of stress granules? In order to examine whether the fifth zinger binds to RNA, we could test RNA-binding ability of PARP-13.2 and compare with insert 8, WWE domain (594-699), and GFP proteins by cross-linked immunoprecipitation (CLIP) assay [73]. Similarly, we can purify the 5^{th} zinc finger alone to test for PAR-binding ability using our established slot blot assay. Another way is to mutate proposed required amino acid for zinc-finger to bind to RNA/PAR, such as cysteine 513 or histidine 531 residues, to see whether the mutation will change stress granule phenotype. By doing so, we could delineate whether the fifth zinc finger is involved on stress granules' regulation.

Concerning about protein overexpression artifact?

Since nearly all data in this study were obtained from protein transfection, we have to ensure that the observed stress granule phenomenon was not caused by overexpression. In order to prevent artifact from protein overexpression, cell images of low-to-medium levels of transient transfection were chosen to quantify and high-levels of cell images should be excluded from analysis [74]. In addition, we have confirmed the FITC channel

analyzed did co-localize with Cy5 channel, which represents stress granule marker, eIF3η. If we would like to control protein expression for the future study, we can make DNA constructs with inducible promoters, which could be turn-on or turn-off by drugs, such as the Tet-On system with doxycycline.

Whether the fragmented phenotype of stress granules could be observed in the absence of eIF2α phosphorylation?

The formation of canonical stress granules was initiated by phosphorylation of eIF2α. We can compare the extent of eIF2α phosphorylation to check whether wild-type PARP-13.2, Y659A, and Q668A display similar ability to form stress granules. Besides, it is studied that the oxidative stress triggered by sodium arsenite will activate heme-regulated inhibitor (HRI) kinase and phosphorylate eIF2α at serine 51 [75]. Since stress granules could be induced by various sources of stress, we would like to investigate whether the fragmented phenotype of stress granules is specific to sodium arsenite. By examining different kinds of stress on transient transfected HeLa (K) cells, such as mitochondria stress, hypoxia, and glucose deprivation, we will know whether the phenotype was not limited to specific stress.

Whether PAR is really essential for stress granule assembly?

In this study, we have identified that ZF-WWE domain of PARP-13 is able to bind to PAR. However, the method cannot prove directly that PAR is essential for stress granule dynamics. In order to test that, we would like to examine the dynamics of stress granule during PAR inhibition by different doses of PARP inhibitors or PAR stabilization

by PARG inhibitor in different time scale. In addition, we would like to use our current PAR binding assay to test whether purified proteins of mutant Y659A and Q668A has weaker binding ability to PAR.

Identify biophysical properties of stress granules

In the 1,6-hexanediol treatment experiment, we found that stress granules of PARP-13.2, Y659A, and Q668A demonstrate different patterns of disassembly under hydrophobic interaction interruption. The distinct biophysical properties of stress granules require more identification. Therefore, we were planning to test biophysical properties of each construct and to compare whether the mutants possess "solid-like" features and the wild-type own "liquid-like" features. In order to observe how stress granules recover after the stimulus and how stress granules interact with each other, live cell imaging and fluorescence recovery after photobleaching (FRAP) would be suitable methods. In our prediction, granules possess liquid properties tend to recover faster than solid ones, since liquid particles tend to exchange component with the surroundings more frequently than solid ones. Also, there are other indicators available to differentiate solid-state particles from liquid-state ones. For example, we can use time-lapse microscopy to observe the behaviors of stress granule formation. The liquid ones are inclined to fuse together over time while the solid ones will remain similar size over the same time scale [63]. The motility of stress granules is another parameter to analyze, that liquid ones usually possess better motility than solid ones, thus we can measure the distance of granules move over time [76].

Identify whether different properties of stress granules affect cell survival

Some apoptotic factors could be recruited to stress granules to prevent cell death [29]. Therefore, we are interested to test whether or not the different pattern of stress granules of PARP-13.2, Y659A, and Q668A contribute to different degrees in preventing apoptosis. We have proposed the WWE mutants possess weaker PAR binding ability than the wild-type WWE; therefore, it is predicted that wild-type WWE could recruit more proteins via protein-PAR-protein interactions. If apoptotic factors were sequestered via the interactions, then it might contribute to different survival between wild-type WWE and mutants. Even though the studied function of WWE domains were on PAR binding, we cannot exclude that WWE could bind to other proteins via protein-protein interaction. In order to test that, we will perform a large-scale immunoprecipitation assay to pull down GFP-PARP-13.2, GFP-Y659A, and GFP-Q668A by GFP-Trap beads, and analyze whether the protein binding partners, such as apoptosis factors, are different by western blots.

In addition, different biophysical properties also influence cell survival. It is known that ALS-linked gene *C9orf72* mutation causes small and abnormal aggregates that solidify stress granules irreversibly, which is toxic to cells [77]. Thus, we are interested to know whether the persistent stress granules of Y659A and Q668A are unfavorable for cell survival. From the process of establishing stable cell expressing wild-type and mutant WWE domains of PARP-13.2, we have noticed that it is faster for GFP-Y659A to lose GFP signals over a few cell passages compared to GFP-PARP-13.2 and GFP-Q668A. Even though the preliminary observation was not confirmed by other

methods yet, it provided us a clue that persistent stress granules might demonstrate different pattern for cell survival as the wild-type PARP-13.2. For future examination, we could select equal number of stable cells of PARP-13.2, Y659A, and Q668A with similar fluorescence intensity by fluorescence-activated cell sorting (FACS), and then seeded them in 24-well plate. We will then harvest the cells at different time points, and monitor how fast the fluorescence diminish with time.

References

1. Anderson, P. and N. Kedersha, *Stress granules.* Curr Biol, 2009. **19**(10): p. R397-8.
2. Decker, C.J. and R. Parker, *P-bodies and stress granules: possible roles in the control of translation and mRNA degradation.* Cold Spring Harb Perspect Biol, 2012. **4**(9): p. a012286.
3. Fan, A.C. and A.K. Leung, *RNA Granules and Diseases: A Case Study of Stress Granules in ALS and FTLD.* Adv Exp Med Biol, 2016. **907**: p. 263-96.
4. Kedersha, N., et al., *Dynamic shuttling of TIA-1 accompanies the recruitment of mRNA to mammalian stress granules.* J Cell Biol, 2000. **151**(6): p. 1257-68.
5. Aulas, A., et al., *Stress-specific differences in assembly and composition of stress granules and related foci.* J Cell Sci, 2017. **130**(5): p. 927-937.
6. Baird, T.D. and R.C. Wek, *Eukaryotic initiation factor 2 phosphorylation and translational control in metabolism.* Adv Nutr, 2012. **3**(3): p. 307-21.
7. Kedersha, N., et al., *Evidence that ternary complex (eIF2-GTP-tRNA(i)(Met))-deficient preinitiation complexes are core constituents of mammalian stress granules.* Mol Biol Cell, 2002. **13**(1): p. 195-210.
8. Svitkin, Y.V., et al., *Eukaryotic translation initiation factor 4E availability controls the switch between cap-dependent and internal ribosomal entry site-mediated translation.* Mol Cell Biol, 2005. **25**(23): p. 10556-65.
9. Mokas, S., et al., *Uncoupling stress granule assembly and translation initiation inhibition.* Mol Biol Cell, 2009. **20**(11): p. 2673-83.
10. Panas, M.D., P. Ivanov, and P. Anderson, *Mechanistic insights into mammalian stress granule dynamics.* J Cell Biol, 2016. **215**(3): p. 313-323.
11. Alves, L.R. and S. Goldenberg, *RNA-binding proteins related to stress response and differentiation in protozoa.* World J Biol Chem, 2016. **7**(1): p. 78-87.
12. Forch, P. and J. Valcarcel, *Molecular mechanisms of gene expression regulation by the apoptosis-promoting protein TIA-1.* Apoptosis, 2001. **6**(6): p. 463-8.
13. Vanderweyde, T., et al., *Role of stress granules and RNA-binding proteins in neurodegeneration: a mini-review.* Gerontology, 2013. **59**(6): p. 524-33.
14. Kedersha, N., P. Ivanov, and P. Anderson, *Stress granules and cell signaling: more than just a passing phase?* Trends Biochem Sci, 2013. **38**(10): p. 494-506.
15. Mamidipudi, V. and C.A. Cartwright, *A novel pro-apoptotic function of RACK1: suppression of Src activity in the intrinsic and Akt pathways.* Oncogene, 2009. **28**(50): p. 4421-33.
16. Piotrowska, J., et al., *Stable formation of compositionally unique stress granules in virus-infected cells.* J Virol, 2010. **84**(7): p. 3654-65.
17. Ohn, T. and P. Anderson, *The role of posttranslational modifications in the assembly of stress granules.* Wiley Interdiscip Rev RNA, 2010. **1**(3): p. 486-93.
18. Tsai, W.C., et al., *Arginine Demethylation of G3BP1 Promotes Stress Granule Assembly.* J Biol Chem, 2016. **291**(43): p. 22671-22685.
19. Reineke, L.C., et al., *Casein Kinase 2 Is Linked to Stress Granule Dynamics through Phosphorylation of the Stress Granule Nucleating Protein G3BP1.* Mol Cell Biol, 2017. **37**(4).

20. Wolozin, B., *Regulated protein aggregation: stress granules and neurodegeneration.* Mol Neurodegener, 2012. **7**: p. 56.
21. Bah, A. and J.D. Forman-Kay, *Modulation of Intrinsically Disordered Protein Function by Post-translational Modifications.* J Biol Chem, 2016. **291**(13): p. 6696-705.
22. Wheeler, J.R., et al., *Distinct stages in stress granule assembly and disassembly.* Elife, 2016. **5**.
23. Jain, S., et al., *ATPase-Modulated Stress Granules Contain a Diverse Proteome and Substructure.* Cell, 2016. **164**(3): p. 487-98.
24. Ohshima, D., et al., *Spatio-temporal Dynamics and Mechanisms of Stress Granule Assembly.* PLoS Comput Biol, 2015. **11**(6): p. e1004326.
25. Alberti, S., et al., *Granulostasis: Protein Quality Control of RNP Granules.* Front Mol Neurosci, 2017. **10**: p. 84.
26. Buchan, J.R., et al., *Eukaryotic stress granules are cleared by autophagy and Cdc48/VCP function.* Cell, 2013. **153**(7): p. 1461-74.
27. Kedersha, N. and P. Anderson, *Stress granules: sites of mRNA triage that regulate mRNA stability and translatability.* Biochem Soc Trans, 2002. **30**(Pt 6): p. 963-9.
28. Sedwick, C., *How stressed cells triage mRNAs.* J Cell Biol, 2015. **211**(5): p. 940.
29. Arimoto, K., et al., *Formation of stress granules inhibits apoptosis by suppressing stress-responsive MAPK pathways.* Nat Cell Biol, 2008. **10**(11): p. 1324-32.
30. Thedieck, K., et al., *Inhibition of mTORC1 by astrin and stress granules prevents apoptosis in cancer cells.* Cell, 2013. **154**(4): p. 859-74.
31. Arimoto-Matsuzaki, K., H. Saito, and M. Takekawa, *TIA1 oxidation inhibits stress granule assembly and sensitizes cells to stress-induced apoptosis.* Nat Commun, 2016. **7**: p. 10252.
32. Miwa, M., et al., *The branching and linear portions of poly(adenosine diphosphate ribose) have the same alpha(1 leads to 2) ribose-ribose linkage.* J Biol Chem, 1981. **256**(6): p. 2916-21.
33. Leidecker, O., et al., *Serine is a new target residue for endogenous ADP-ribosylation on histones.* Nat Chem Biol, 2016. **12**(12): p. 998-1000.
34. Krietsch, J., et al., *Reprogramming cellular events by poly(ADP-ribose)-binding proteins.* Mol Aspects Med, 2013. **34**(6): p. 1066-87.
35. Luo, X. and W.L. Kraus, *On PAR with PARP: cellular stress signaling through poly(ADP-ribose) and PARP-1.* Genes Dev, 2012. **26**(5): p. 417-32.
36. Leung, A.K., *Poly(ADP-ribose): an organizer of cellular architecture.* J Cell Biol, 2014. **205**(5): p. 613-9.
37. Teloni, F. and M. Altmeyer, *Readers of poly(ADP-ribose): designed to be fit for purpose.* Nucleic Acids Res, 2016. **44**(3): p. 993-1006.
38. Vyas, S., et al., *Family-wide analysis of poly(ADP-ribose) polymerase activity.* Nat Commun, 2014. **5**: p. 4426.
39. Gibson, B.A. and W.L. Kraus, *New insights into the molecular and cellular functions of poly(ADP-ribose) and PARPs.* Nat Rev Mol Cell Biol, 2012. **13**(7): p. 411-24.

40. Feijs, K.L., P. Verheugd, and B. Luscher, *Expanding functions of intracellular resident mono-ADP-ribosylation in cell physiology.* FEBS J, 2013. **280**(15): p. 3519-29.
41. Karlberg, T., et al., *Structural basis for lack of ADP-ribosyltransferase activity in poly(ADP-ribose) polymerase-13/zinc finger antiviral protein.* J Biol Chem, 2015. **290**(12): p. 7336-44.
42. Kleine, H., et al., *Substrate-assisted catalysis by PARP10 limits its activity to mono-ADP-ribosylation.* Mol Cell, 2008. **32**(1): p. 57-69.
43. Barkauskaite, E., et al., *The recognition and removal of cellular poly(ADP-ribose) signals.* FEBS J, 2013. **280**(15): p. 3491-507.
44. Niere, M., et al., *ADP-ribosylhydrolase 3 (ARH3), not poly(ADP-ribose) glycohydrolase (PARG) isoforms, is responsible for degradation of mitochondrial matrix-associated poly(ADP-ribose).* J Biol Chem, 2012. **287**(20): p. 16088-102.
45. Fontana, P., et al., *Serine ADP-ribosylation reversal by the hydrolase ARH3.* Elife, 2017. **6**.
46. Kim, M.Y., T. Zhang, and W.L. Kraus, *Poly(ADP-ribosyl)ation by PARP-1: 'PAR-laying' NAD+ into a nuclear signal.* Genes Dev, 2005. **19**(17): p. 1951-67.
47. Althaus, F.R., et al., *Poly ADP-ribosylation: a DNA break signal mechanism.* Mol Cell Biochem, 1999. **193**(1-2): p. 5-11.
48. Gagne, J.P., et al., *Proteome-wide identification of poly(ADP-ribose) binding proteins and poly(ADP-ribose)-associated protein complexes.* Nucleic Acids Res, 2008. **36**(22): p. 6959-76.
49. Ahel, I., et al., *Poly(ADP-ribose)-binding zinc finger motifs in DNA repair/checkpoint proteins.* Nature, 2008. **451**(7174): p. 81-5.
50. Karras, G.I., et al., *The macro domain is an ADP-ribose binding module.* EMBO J, 2005. **24**(11): p. 1911-20.
51. Rosenthal, F., et al., *Macrodomain-containing proteins are new mono-ADP-ribosylhydrolases.* Nat Struct Mol Biol, 2013. **20**(4): p. 502-7.
52. Aravind, L., *The WWE domain: a common interaction module in protein ubiquitination and ADP ribosylation.* Trends Biochem Sci, 2001. **26**(5): p. 273-5.
53. Wang, Z., et al., *Recognition of the iso-ADP-ribose moiety in poly(ADP-ribose) by WWE domains suggests a general mechanism for poly(ADP-ribosyl)ation-dependent ubiquitination.* Genes Dev, 2012. **26**(3): p. 235-40.
54. Vyas, S., et al., *A systematic analysis of the PARP protein family identifies new functions critical for cell physiology.* Nat Commun, 2013. **4**: p. 2240.
55. Leung, A.K., et al., *Poly(ADP-ribose) regulates stress responses and microRNA activity in the cytoplasm.* Mol Cell, 2011. **42**(4): p. 489-99.
56. Liu, C. and X. Yu, *ADP-ribosyltransferases and poly ADP-ribosylation.* Curr Protein Pept Sci, 2015. **16**(6): p. 491-501.
57. Todorova, T., F.J. Bock, and P. Chang, *PARP13 regulates cellular mRNA post-transcriptionally and functions as a pro-apoptotic factor by destabilizing TRAILR4 transcript.* Nat Commun, 2014. **5**: p. 5362.
58. Leung, A., et al., *Poly(ADP-ribose) regulates post-transcriptional gene regulation in the cytoplasm.* RNA Biol, 2012. **9**(5): p. 542-8.

59. Tan, E.S., K.A. Krukenberg, and T.J. Mitchison, *Large-scale preparation and characterization of poly(ADP-ribose) and defined length polymers.* Anal Biochem, 2012. **428**(2): p. 126-36.
60. Anderson, P. and N. Kedersha, *RNA granules.* J Cell Biol, 2006. **172**(6): p. 803-8.
61. Spector, D.L., *SnapShot: Cellular bodies.* Cell, 2006. **127**(5): p. 1071.
62. Zweifel, M.E., D.J. Leahy, and D. Barrick, *Structure and Notch receptor binding of the tandem WWE domain of Deltex.* Structure, 2005. **13**(11): p. 1599-611.
63. Kroschwald, S., et al., *Promiscuous interactions and protein disaggregases determine the material state of stress-inducible RNP granules.* Elife, 2015. **4**: p. e06807.
64. Uchima, L. and Massachusetts Institute of Technology. Department of Biology., *Farnesylation-dependent regulation of transcripts by PARP13*. 2015. 152 pages.
65. Charron, G., et al., *Prenylome profiling reveals S-farnesylation is crucial for membrane targeting and antiviral activity of ZAP long-isoform.* Proc Natl Acad Sci U S A, 2013. **110**(27): p. 11085-90.
66. Welsby, I., et al., *PARP12, an interferon-stimulated gene involved in the control of protein translation and inflammation.* J Biol Chem, 2014. **289**(38): p. 26642-57.
67. Zhang, Y., et al., *RNF146 is a poly(ADP-ribose)-directed E3 ligase that regulates axin degradation and Wnt signalling.* Nat Cell Biol, 2011. **13**(5): p. 623-9.
68. He, F., et al., *Structural insight into the interaction of ADP-ribose with the PARP WWE domains.* FEBS Lett, 2012. **586**(21): p. 3858-64.
69. Zhang, H., et al., *RNA Controls PolyQ Protein Phase Transitions.* Mol Cell, 2015. **60**(2): p. 220-30.
70. Patel, A., et al., *A Liquid-to-Solid Phase Transition of the ALS Protein FUS Accelerated by Disease Mutation.* Cell, 2015. **162**(5): p. 1066-77.
71. Brangwynne, C.P., P. Tompa, and R.V. Pappu, *Polymer physics of intracellular phase transitions.* Nature Physics, 2015. **11**(11): p. 899-904.
72. Mateju, D., et al., *An aberrant phase transition of stress granules triggered by misfolded protein and prevented by chaperone function.* EMBO J, 2017. **36**(12): p. 1669-1687.
73. Ule, J., et al., *CLIP: A method for identifying protein–RNA interaction sites in living cells*. Methods, 2005. **37**(4): p. 376-86
74. Aulas, A., et al., *G3BP1 promotes stress-induced RNA granule interactions to preserve polyadenylated mRNA.* J Cell Biol, 2015. **209**(1): p. 73-84.
75. McEwen, E., et al., *Heme-regulated inhibitor kinase-mediated phosphorylation of eukaryotic translation initiation factor 2 inhibits translation, induces stress granule formation, and mediates survival upon arsenite exposure.* J Biol Chem, 2005. **280**(17): p. 16925-33.
76. Gopal, P.P., et al., *Amyotrophic lateral sclerosis-linked mutations increase the viscosity of liquid-like TDP-43 RNP granules in neurons.* Proc Natl Acad Sci U S A, 2017. **114**(12): p. E2466-E2475.
77. Boeynaems, S., et al., *Phase Separation of C9orf72 Dipeptide Repeats Perturbs Stress Granule Dynamics.* Mol Cell, 2017. **65**(6): p. 1044-1055 e5.

Curriculum Vitae

Shang-Jung Cheng 鄭上容
501 Saint Paul St. Apt 210 • Baltimore, MD 21202 • (818) 751-9041 •
scheng32@jhu.edu

EDUCATION

Johns Hopkins University
Bloomberg School of Public Health, Department of Biochemistry and Molecular Biology
Master of Science, August 2017 (expected)
ScM thesis:
How does the WWE domain of PARP13 regulate the assembly of stress granules?
MHS thesis: Stemness maintenance in breast cancer stem cells
Cumulative GPA: 3.86

National Taiwan University
College of Medicine, Graduate Institute of Physiology
Master of Science, June 2010; rank: 3/15
Thesis: The Effect of Arachidonic Acid on TNF-α-induced NF-κB signaling studied in human breast cancer cell line and rat mammary tumors

National Taiwan University
College of Bio-Resources and Agriculture, Department of Agricultural Chemistry
College of Public Health, Department of Public Health (double-major)
Bachelor of Science, June 2008; rank: 5/40

RESEARCH EXPERIENCE

Johns Hopkins University
Department of Biochemistry and Molecular Biology Jan 2016 – present
MHS/ScM graduate student
PI: Dr. Anthony K.L. Leung
Investigate how PARP13 regulates the assembly of stress granules by immunofluorescence/microscopy, purify protein and perform *in vitro* and *in vivo* PAR binding assay; prepared common buffer and bacteria competent cells for the lab

Academia Sinica, Institute of Biomedical Sciences May – Jun 2015
Research Assistant
PI: Dr. Te-Chang Lee
Studied mechanism of natural antioxidants on translocation of Rad51 in H460 lung cancer cells

Academia Sinica, Institute of Biomedical Sciences July 2012 – Apr 2015
Research Assistant
PI: Dr. Sheau-Yann Shieh
Explored effects of BTG3 on angiogenesis via HIF-1-α pathway; examined effects of Trim-17 sumoylation on cell cycle, including preparing DNA construct, operating flow cytometry, and collecting TCGA data to do Kaplan-Meier analysis; prepared common buffer/chemical reagents and bacteria competent cells for the lab

National Taiwan University, Institute of Physiology July 2010 – Dec 2010
Sep 2011 – Apr 2012
Research Assistant
PI: Dr. Hui-Min Su
Investigate how long-term-estradiol-deprivation (LTED) alters signaling on MCF-7 human breast cancer cell; instructed new students on essential laboratory skills (cell culture, electrophoresis)

INTERNSHIP

Clinical Trial Center, National Taiwan University Hospital Jul – Aug 2008
Intern
Familiarized with procedures and regulations of clinical research and observed ongoing clinical trials on application of aural acupuncture as a form to soothe breast cancer patients' side-effects from chemotherapy.

TEACHING EXPERIENCE

National Taiwan University, Institute of Physiology Spring, 2009
Teaching assistant
Prepared the lab prior to each session and assisted medical students with lab works in Human Physiology class

HONOR

National Taiwan University Presidential Award 2008
(Top 5% on coursework in the class, 2008)

The Second Annual National Taiwan University, School of Medicine Writing Competition, honorable mentioned 2009

PUBLICATIONS

R.L. McPherson, R. Abraham, E. Sreekumar, S.E. Ong, S.J. Cheng, V.K. Baxter, H.A.V. Kistemaker, D.V. Filippov, D.E. Griffin & A.K.L. Leung.
"ADP-ribosylhydrolase activity of Chikungunya virus macrodomain is critical for virus replication and virulence." *PNAS, 2017*

H.W. Chang, S.J. Cheng, H.Y. Chiang & S.Y. Shieh.
"Functional characterization of the BTG3 ablation-associated secretory phenotype in tumorigenesis." (Under preparation)

Y.C. Cheng, F.F. Hsu, S.J. Cheng & S.Y. Shieh.
"TRIM-17 functions as a CHK1 SUMO E3 ligase to promote CHK1 nuclear exclusion." (Under preparation)

PRESENTATIONS

S.J. Cheng & A.K.L. Leung.
Departmental retreat, Gettysburg. Oral presentation. 2017
How does the WWE domain of PARP13 regulate the assembly of stress granules?

S.J. Cheng & H.M. Su. 2012
Tenth Congress of the International Society for the Study for Fatty Acids and Lipids (ISSFAL). Vancouver, Canada. Chosen Oral presentation.
Arachidonic acid enhances TNF-α-induced NF-κB signaling studied in human breast cancer cell line and rat mammary tumors.

RESEARCH SKILLS

Analytical Chemistry: Laser Scanning Confocal Microscopy (Leica SP5), DeltaVision Deconvolution Microscopy, Fast Protein Liquid Chromatography (FPLC)

Biochemistry and Molecular Biology: Cell culture, Western Blot, Immunofluorescence, Electrophoretic mobility shift assay (EMSA), Flow cytometry, Pull-down assay, cytokine array, Luciferase assay, DNA cloning, PCR, protein purification

Animal experiment: Intravenous (IV) anaesthesia and Femoral artery (vein) catheterization in rat, dissecting, extracting and analyzing rat mammary tumors

Data analysis software: ImageJ (quantification), Excel, Prism, JMP (plot and basic statistics), R (basic statistics)

LANGUAGE

Mandarin Chinese (native), English (fluent)